Article

SOURCE DATA | TRANSPARENT PROCESS | OPEN ACCESS

EMBO reports

Promyelocytic leukemia protein targets MK2 to promote cytotoxicity

I-Ting Chen[1], Hsiao-Chi Chen[1], Yu-Hsun Lo[1], Peng-Yeh Lai[1], Fu-Yi Hsieh[1], Yung-Hsuan Wu[1], Hsiu-Ming Shih[2] & Ming-Zong Lai[1,*]

Abstract

Promyelocytic leukemia protein (PML) is a tumor suppressor possessing multiple modes of action, including induction of apoptosis. We unexpectedly find that PML promotes necroptosis in addition to apoptosis, with *Pml*$^{-/-}$ macrophages being more resistant to TNF-mediated necroptosis than wild-type counterparts and PML-deficient mice displaying resistance to TNF-induced systemic inflammatory response syndrome. Reduced necroptosis in PML-deficient cells is associated with attenuated receptor-interacting protein kinase 1 (RIPK1) activation, as revealed by reduced RIPK1 [S166] phosphorylation, and attenuated RIPK1-RIPK3-MLKL necrosome complex formation. We show that PML deficiency leads to enhanced TNF-induced MAPK-activated kinase 2 (MK2) activation and elevated RIPK1[S321] phosphorylation, which suppresses necrosome formation. MK2 inhibitor treatment or MK2 knockout abrogates resistance to cell death induction in PML-null cells and mice. PML binds MK2 and p38 MAPK, thereby inhibiting p38-MK2 interaction and MK2 activation. Moreover, PML participates in autocrine production of TNF induced by cellular inhibitors of apoptosis 1 (cIAP1)/cIAP2 degradation, since PML-knockout attenuates autocrine TNF. Thus, by targeting MK2 activation and autocrine TNF, PML promotes necroptosis and apoptosis, representing a novel tumor-suppressive activity for PML.

Keywords MK2; necroptosis; p38 MAPK; PML; RIPK1
Subject Categories Autophagy & Cell Death; Cancer; Signal Transduction
DOI 10.15252/embr.202052254 | Received 10 December 2020 | Revised 19 September 2021 | Accepted 27 September 2021 | Published online 11 October 2021
EMBO Reports (2021) 22: e52254

Introduction

Promyelocytic leukemia protein (PML) is a tumor suppressor that regulates cell growth, cell cycle control, transcription, apoptosis, stress responses, epigenetic control, antiviral reactivity, senescence, telomere elongation, and stem cell renewal (Salomoni & Pandolfi, 2002; Bernardi & Pandolfi, 2007; Niwa-Kawakita *et al*, 2017). PML is essential for the formation of PML nuclear bodies (PML NBs), where Sp100, Daxx, p53, Rb, small ubiquitin-like modifier (SUMO-1), and breast cancer-1 (BRCA-1) co-localize (Bernardi & Pandolfi, 2007; Lallemand-Breitenbach & de The, 2018). The human *PML* gene comprises nine exons. Alternative splicing of the *PML* gene generates at least seven PML isoforms with different C-terminal segments, but they share common N-terminal regions harboring a really interesting new gene finger, B-boxes, and a coiled-coil domain (RBCC) region (Condemine *et al*, 2006; Maarifi *et al*, 2014). PML is down-regulated in several types of tumors (Gurrieri *et al*, 2004). The tumor suppressor activity of PML can be partly attributed to its regulation of p53 activity, suppression of PI3K-mTOR, and ability to promote cell death. PML promotes apoptosis induced by p53, tumor necrosis factor (TNF), Fas, and interferons (IFNs) (Wang *et al*, 1998; Bernardi *et al*, 2008; Hsu *et al*, 2016). It also participates in NLRP3 inflammasome activation that leads to pyroptotic death (Lo *et al*, 2013).

Recent studies have revealed that PML NBs are liquid-like droplets having an outer shell of oligomerized PML proteins that serve as scaffolds for recruiting partner proteins and clients, mostly in a SUMO-dependent manner (Sahin *et al*, 2014; Banani *et al*, 2016; Lallemand-Breitenbach & de The, 2018). It is generally believed that PML NBs act as a platform for PML-binding proteins undergoing post-translational modification, especially SUMOylation. In addition, PML NBs serve as a scaffold that regulates cellular function by sequestering PML-interacting proteins. One mechanism by which PML exerts its regulatory action is by sequestering suppressors or activators in the nucleus. Nuclear sequestration of Daxx by PML prevents Daxx-mediated transcription (Li *et al*, 2000; Lin *et al*, 2003). PML regulates p53-induced death partly by sequestering MDM2 in the nucleolus and enhancing p53 stability (Bernardi *et al*, 2004). Mad1 destabilizes p53 by interfering with PML-directed sequestration of MDM2 (Wan *et al*, 2019). Recruitment of IKKε into PML NBs also confers resistance to DNA-damage-induced death (Renner *et al*, 2010). Notably, cytoplasmic PML isoforms (Lin *et al*, 2004; Condemine *et al*, 2006) regulate cell death and other processes. Cytoplasmic PML has also been shown to inhibit p53 function (Bellodi *et al*, 2006), and extranuclear PML localized at ER and mitochondria-associated membranes controls calcium influx and regulates ER stress-induced apoptosis (Giorgi *et al*, 2010).

Necroptotic cell death participates in inflammation, tumorigenesis, control of viral infection, and the pathogenesis of several

1 Institute of Molecular Biology, Taipei, Taiwan
2 Institute of Biomedical Sciences, Academia Sinica, Taipei, Taiwan
*Corresponding author. Tel: +886 2 2789 9236; Fax: +886 2 2782 6085, +886 2 2782 7784; E-mail: mblai@gate.sinica.edu.tw

diseases (Robinson *et al*, 2012; Chan *et al*, 2015; Pasparakis & Vandenabeele, 2015; Wallach *et al*, 2016; Weinlich *et al*, 2017; Annibaldi & Meier, 2018; Galluzzi *et al*, 2018). During TNF-mediated necroptosis, cell death is initiated by the activation of receptor-interacting protein kinase 1 (RIPK1)-RIPK3 and suppression of FADD-caspase-8 activity. TNF receptor engagement induces ligation of RIPK1 to K63 or M1 linear polyubiquitin chains by, respectively, E3 ligase cellular inhibitors of apoptosis 1 (cIAP1)/cIAP2 or linear ubiquitin chain assembly complex (LUBAC) (Bertrand *et al*, 2008; Mahoney *et al*, 2008; Varfolomeev *et al*, 2008; Gerlach *et al*, 2011; Ikeda *et al*, 2011). RIPK1 polyubiquitination chains serve as signaling backbones for assembling and activating IκB kinase (IKK) complexes and for NF-κB activation, as well as recruitment of TAK1 for p38 MAPK cascade activation. Removal of RIPK1 signaling polyubiquitination, for example, by depletion of cIAP1/2, leads to association of RIPK1 with FADD and caspase-8 and inactivation cleavage of RIPK1 by caspase-8. Genetic or biochemical suppression of caspase-8 enables RIPK1 to form a necroptotic complex by binding RIPK3 and inducing RIPK3 autophosphorylation (Cho *et al*, 2009; He *et al*, 2009; Zhang *et al*, 2009). Activated RIPK3 then phosphorylates and induces mixed lineage kinase domain-like (MLKL) activity (Sun *et al*, 2012; Zhao *et al*, 2012), resulting in translocation of phosphorylated MLKL into plasma membranes for pore formation and necroptosis (Murphy *et al*, 2013; Cai *et al*, 2014; Chen *et al*, 2014; Hildebrand *et al*, 2014; Wang *et al*, 2014). The pivotal role of RIPK1 and RIPK3 in necroptosis is best demonstrated by the fact that deletion of either RIPK1 or RIPK3 prevents embryonic death caused by deficiency of FADD, caspase-8, or c-FLIP (Kaiser *et al*, 2011; Oberst *et al*, 2011; Zhang *et al*, 2011). In addition, the kinase activity of RIPK, often illustrated by S166 autophosphorylation (Degterev *et al*, 2008), initiates TNF-dependent necroptosis by inducing RIPK3 phosphorylation. Experimentally, degradation of cIAP1/2 by mimetics of second mitochondria-derived activator of caspases (SMAC), combined with inhibition of caspase-8 by the pan-caspase-inhibitor zVAD, is an approach often used to induce necroptosis. RIPK1 also exhibits a specific role in limiting necroptosis and apoptosis, as well as inhibition of cell death-associated inflammation (Dillon *et al*, 2014; Kaiser *et al*, 2014; Rickard James *et al*, 2014).

MAPK-activated kinase 2 (MAPKAPK2, MK2) is a major signaling pathway that operates downstream of p38 MAPK (Menon & Gaestel, 2018; Han *et al*, 2020). MK2 and p38 MAPK are activated in the nucleus, where MKK3 also phosphorylates p38 MAPK (Ben-Levy *et al*, 1998; Engel *et al*, 1998). Activated p38 MAPK then phosphorylates MK2, enabling it to enter the cytoplasm (Ben-Levy *et al*, 1998; Engel *et al*, 1998; Shin *et al*, 2004). There, MK2 phosphorylates tristetraprolin (TTP), inhibiting TTP from destabilizing mRNA (Hitti *et al*, 2006) and thereby enhancing expression of inflammatory cytokines. Importantly, MK2 inhibits necroptosis via direct phosphorylation of RIPK1 at residues S321 and S326, which prevents RIPK1 activation (marked by reduced phosphorylation of RIPK1 at residue S166) (Jaco *et al*, 2017; Menon *et al*, 2017) and attenuates binding of RIPK1 to FADD-caspase-8 (Dondelinger *et al*, 2017; Jaco *et al*, 2017; Menon *et al*, 2017). Accordingly, MK2 is now recognized as a therapeutic target in inflammation, cancer, and neurodegeneration (Menon & Gaestel, 2018).

In the present study, we found that PML can promote necroptosis. PML deficiency led to diminished necroptosis and apoptosis. We further reveal that PML inhibits p38-MK2 interaction, and PML deficiency results in enhanced activation of p38 MAPK and MK2, thereby increasing MK2-directed necrosome-inhibitory S321 phosphorylation of RIPK1. In addition, PML participates in autocrine production of TNF induced by cIAP1/2 degradation. Our results demonstrate that promotion of necroptosis constitutes a previously unknown tumor suppressor activity of PML. Moreover, PML may represent a new therapeutic target for MK2-mediated inflammation.

Results

Attenuation of TNF-mediated necroptosis in PML-deficient macrophages and HT-29 cells

We used bone marrow-derived macrophages (BMDMs) generated from wild-type control and *Pml*$^{-/-}$ mice to evaluate whether PML affected necroptosis. Treatment of BMDMs with the pan-caspase inhibitor zVAD did not affect the viability of macrophages, as measured by ATP release (Fig 1A). A combination of zVAD and the second mitochondria-derived activator of caspases (SMAC) mimetic AT-406 induced cell death in BMDMs (Fig 1A). Unexpectedly, we found that PML-deficient BMDMs were more resistant to cell death induced by zVAD + AT-406 than WT BMDMs (Fig 1A). The necroptotic nature of the cell death induced by zVAD/SMAC mimetic treatment is demonstrated by the cell death being fully suppressed upon inclusion of the RIPK1 inhibitor necrostatin-1 (Nec-1) or the RIPK3 inhibitor GSK872 (Fig 1A). Necroptosis could also be induced by TNF plus zVAD, shown by its sensitivity to inhibition by Nec-1 or GSK872, whereas PML deficiency conferred resistance to macrophage death triggered by TNF + zVAD (Fig 1B). The difference in necroptosis between WT and *Pml*$^{-/-}$ BMDMs was not due to a difference in expression of necroptosis-execution molecules, as levels of RIPK1, RIPK3, and MLKL were comparable between control and *Pml*$^{-/-}$ BMDMs (Fig 1C). Similar to BMDMs, *Pml*$^{-/-}$ mouse embryonic fibroblasts (MEFs) were resistant to necroptosis induction by TNF+ zVAD, relative to WT MEFs (Fig 1D).

We observed a similar protective effect against necroptosis imposed by PML deficiency in the human pro-monocytic cell line U937 and the human colon adenocarcinoma cell line HT-29. Necroptotic cell death induced by TNF + AT-406 + zVAD in the U937 cell line was blocked by inhibition of RIPK1 or RIPK3, and it was attenuated by PML knockout (Appendix Fig S1A). HT-29 cells have been reported for their susceptibility to necroptosis (He *et al*, 2009). In the presence of increasing doses of TNF, treatment of WT HT-29 cells with zVAD + BV6 (another SMAC mimetic) triggered significant cell death which was suppressed by Nec-1 (Appendix Fig S1B). PML downregulation, either via knockdown by shRNA or knockout by CRISPR-Cas9 editing, limited the necroptosis induced by zVAD + BV6 + TNF in HT-29 cells (Appendix Fig S1B and C). Together, these results demonstrate that PML deficiency suppresses TNF-triggered necroptosis, indicating that PML participates in necroptosis. The specificity of PML was further confirmed by the re-introduction of PML into PML-deficient primary MEFs conferring the sensitivity to necroptosis induction (Appendix Fig S1D and E).

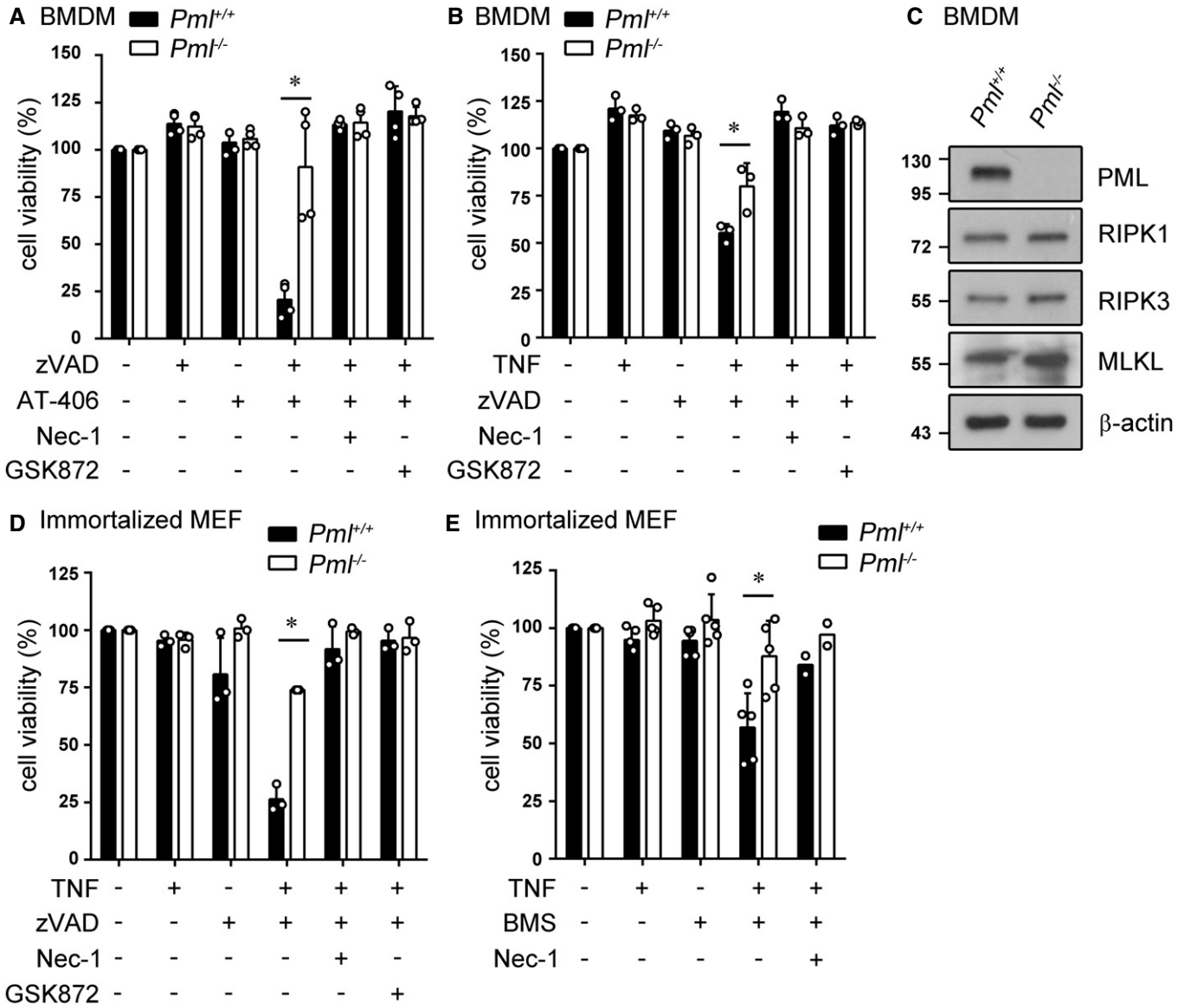

Figure 1. PML deficiency inhibits necroptosis and apoptosis induction in BMDMs and MEFs.

A BMDMs from WT (*Pml*$^{+/+}$) and *Pml*$^{-/-}$ mice were pre-treated with zVAD (20 μM), Nec-1 (40 μM), or GSK872 (10 μM), as indicated, for 30 min followed by co-treatment with AT-406 (1 μM). Cell viability was evaluated by ATP release after 18 h. Data show mean ± SD of four biological replicates.

B WT and *Pml*$^{-/-}$ BMDM were treated with TNF (100 ng/ml), zVAD (20 μM), and Nec-1 (40 μM) or GSK872 (10 μM), as indicated, for 16 h. Cell viability was determined by ATP release. Data show mean ± SD of three biological replicates.

C Normal expression of RIPK1, RIPK3, and MLKL in *Pml*$^{-/-}$ BMDMs. Lysates from WT and *Pml*$^{-/-}$ BMDMs were analyzed for their levels of RIPK1, RIPK3, and MLKL.

D WT and *Pml*$^{-/-}$ immortalized MEFs were treated with TNF (100 ng/ml), zVAD (20 μM), Nec-1 (40 μM), and GSK872 (10 μM), as indicated, for 8 h. Cell viability was determined by ATP assay. Data show mean ± SD of three biological replicates.

E WT and *Pml*$^{-/-}$ immortalized MEFs were treated with TNF (100 ng/ml), IKK inhibitor BMS-345541 (10 mM) and Nec-1, as indicated, for 6 h, and then, cell death was assayed. Data show mean ± SD of five biological replicates, except the Nec-1-containing experiment ($n = 2$).

Data information: *$P < 0.05$ for multiple *t*-tests according to the Holm–Sidak method (A, B, D, E).
Source data are available online for this figure.

Since RIPK1 also mediates TNF-induced apoptosis, we examined whether TNF-initiated apoptosis was also affected by PML deficiency. Apoptosis triggered by TNF plus the IKK inhibitor BMS-345541 in WT MEFs was prevented in *Pml*$^{-/-}$ MEFs (Fig 1E), as also illustrated by reduced cleavage of caspase-8 (Appendix Fig S2A). Notably, apoptosis and caspase-3 activation induced by TNF + cycloheximide (CHX), which is RIPK1-independent (Dondelinger *et al*, 2013), was nearly undetectable in *Pml*$^{-/-}$ MEFs (Appendix Fig S2B and C). Therefore, PML deficiency inhibits RIPK1-mediated necroptosis and apoptosis, as well as RIPK1-independent apoptosis.

PML deficiency reduces phosphorylation of RIPK1[S166], RIPK3, and MLKL

During TNF-initiated necrotic signaling, RIPK1 kinase is activated upon residue S166 autophosphorylation (Degterev *et al*, 2008). Phosphorylated RIPK1 (p-RIPK1) promotes RIPK3 autophosphorylation that, in turn, phosphorylates MLKL to trigger cell death. Treatment of BMDMs with zVAD + AT-406 induced activation of RIPK1, RIPK3, and MLKL (Fig 2A). We observed diminished phosphorylation (relative to WT BMDMs) of RIPK1[S166], RIPK3, and MLKL in $Pml^{-/-}$ BMDMs after treatment with zVAD + AT-406 (Fig 2A). Quantitation from three independent experiments (biological replicates) indicates a significant reduction of p-RIPK1[S166] at 4 and 6 h after necroptosis induction (Fig 2A). Notably, 6 h after zVAD + AT-406 treatment, there was a clear decrease in the amounts of RIPK1, RIPK3, and MLKL in WT BMDMs (Fig 2A), reflecting extensive cell death by that time-point. Treatment of $Pml^{-/-}$ BMDMs with TNF + zVAD also led to reduced phosphorylation of RIPK1[S166], RIPK3, and MLKL (Fig 2B). Attenuated phosphorylation (relative to WT HT-29 cells) of RIPK1[S166], RIPK3, and MLKL was also found in PML-knockdown HT-29 cells after zVAD + BV6 + TNF treatment (Appendix Fig S3A–C). Consistent with reduced necroptosis, we recorded diminished activation of the RIPK1-RIPK3-MLKL axis in PML-deficient HT-29 cells. Therefore, PML deficiency inhibits induction of necroptosis in both macrophages and HT-29 cells by suppressing pro-necroptotic phosphorylation of RIPK1, RIPK3, and MLKL.

The impact of PML deficiency on necroptosis in macrophages was greater for the zVAD +AT-406 than TNF + zVAD treatment (Figs 1A and B, and 2A and B). We examined whether the presence of the SMAC mimetic AT-406 contributed to that discrepancy. High concentrations of AT-406 (> 5 μM) alone induced apoptosis (Fig 2C), as previously documented (Varfolomeev *et al*, 2007; Vince *et al*, 2007), but the dose of AT-406 (1 μM) used in the present study (Figs 1 and 2) alone did not trigger cell death (Fig 2C). SMAC mimetics are known to induce TNF by cIAP1/2 degradation (Varfolomeev *et al*, 2007; Vince *et al*, 2007), zVAD +AT-406 triggered TNF production in WT macrophages (Fig 2D), and TNF neutralization by antibodies prevented cell death (Fig 2E). However, we found that autocrine TNF in $Pml^{-/-}$ BMDMs was largely reduced (Fig 2D), suggesting that diminished TNF induction by zVAD +AT-406 contributes to their resistance to necroptosis. These results also suggest that the reduced impact of PML deficiency on the necroptosis induced by TNF + zVAD treatment is likely due to lack of an effect on autocrine TNF.

Reduced necroptosome assembly in PML-deficient cells

TNF-induced necroptosome formation is initiated by binding of RIPK1 to FADD and caspase-8. Immunoprecipitation of FADD brought down p-RIPK1[S166], RIPK1, and caspase-8 from BMDMs treated with zVAD + AT-406 (Fig 3A), and this association of p-RIPK1[S166], RIPK1, and caspase-8 with FADD was diminished in $Pml^{-/-}$ macrophages (Fig 3A). Similarly, the quantities of p-RIPK1 [S166] and RIPK1 pulled down with caspase-8 were reduced in $Pml^{-/-}$ macrophages subjected to the same treatment (Fig 3B). A comparable effect of PML deficiency was found for HT-29 cells, since stimulation of HT-29 cells with zVAD + BV6 + TNF led to a reduced association of FADD with RIPK1, RIPK3, caspase-8, and MLKL in PML-knockdown cells (Appendix Fig S3D). Therefore, PML deficiency inhibits formation of the FADD-caspase-8-RIPK1-RIPK3-MLKL complex.

Resistance to TNF-induced septic shock in PML-null mice

Next, we examined whether PML deficiency affects necroptosis-associated events *in vivo*. TNF-induced systemic inflammatory response syndrome is mediated by necroptosis and apoptosis and is dependent on RIPK1 and RIPK3 (Duprez *et al*, 2011; Polykratis *et al*, 2014; Newton *et al*, 2016). We found that TNF administration induced hypothermia and death in WT mice (Fig 4A and B). However, PML-null mice were fully protected from severe hypothermia and TNF-induced lethality (Fig 4A and B). In addition, TNF-induced inflammation, marked by elevated serum levels of lactic dehydrogenase (LDH) and glutamate pyruvate transaminase/alanine aminotransferase (GPT/ALT) in WT mice, was strongly suppressed in $Pml^{-/-}$ mice (Fig 4C and D). Consistent with $Pml^{-/-}$ mouse resistance to TNF-induced hypothermia, such mice displayed reduced serum levels of TNF (Fig 4E), and a marginal decrease in serum contents of IL-6 and IL-1α (Fig 4F and G). Therefore, PML deficiency confers resistance to necroptosis and apoptosis in both cultured cells and live animals, accompanied by lowered inflammatory cytokine generation *in vivo*.

PML deficiency increases MK2-mediated phosphorylation of RIPK1 at S321

We then examined how PML regulates the formation of the RIPK1-containing pro-necroptotic complex. Recent studies have revealed that TNF receptor downstream signaling regulates RIPK1-containing necrosome formation via several different pathways. Phosphorylation of RIPK1 by IKKα/IKKβ prevents RIPK1-initiated necroptosis

Figure 2. Attenuated phosphorylation of RIPK1[S166], RIPK3, and MLKL in PML-deficient cells following necroptosis induction.

A, B $Pml^{+/+}$ and $Pml^{-/-}$ BMDMs were treated with zVAD + AT-406 (zA) (A) or TNF + zVAD (Tz) (B), as in Fig 1, for the indicated times. Contents of RIPK1, p-RIPK1[S166], RIPK3, p-RIPK3, MLKL, and p-MLKL in cell lysates were analyzed by immunoblots. Bottom panels, quantitation of p-RIPK1[S166] from three biological replicates using normalized intensity of p-RIPK1[S166] in WT cells at 4 h as 1. Data show mean ± SD.

C $Pml^{+/+}$ and $Pml^{-/-}$ BMDMs were treated with AT-406 at the concentration indicated for 24 h, and cell viability was then determined by ATP assay. Data show mean ± SD of three biological replicates.

D BMDMs were treated with zVAD (20 μM) +AT-406 (1 μM) for 18 h, and TNF generated was then analyzed by ELISA. Data show mean ± SD of four biological replicates.

E BMDMs were treated with zVAD + AT-406 (1 μM), with or without anti-TNF for 18 h, and cell viability quantitated. Data show mean ± SD of three biological replicates.

Data information: *$P < 0.05$ for multiple *t*-tests according to the Holm–Sidak method (A–E).
Source data are available online for this figure.

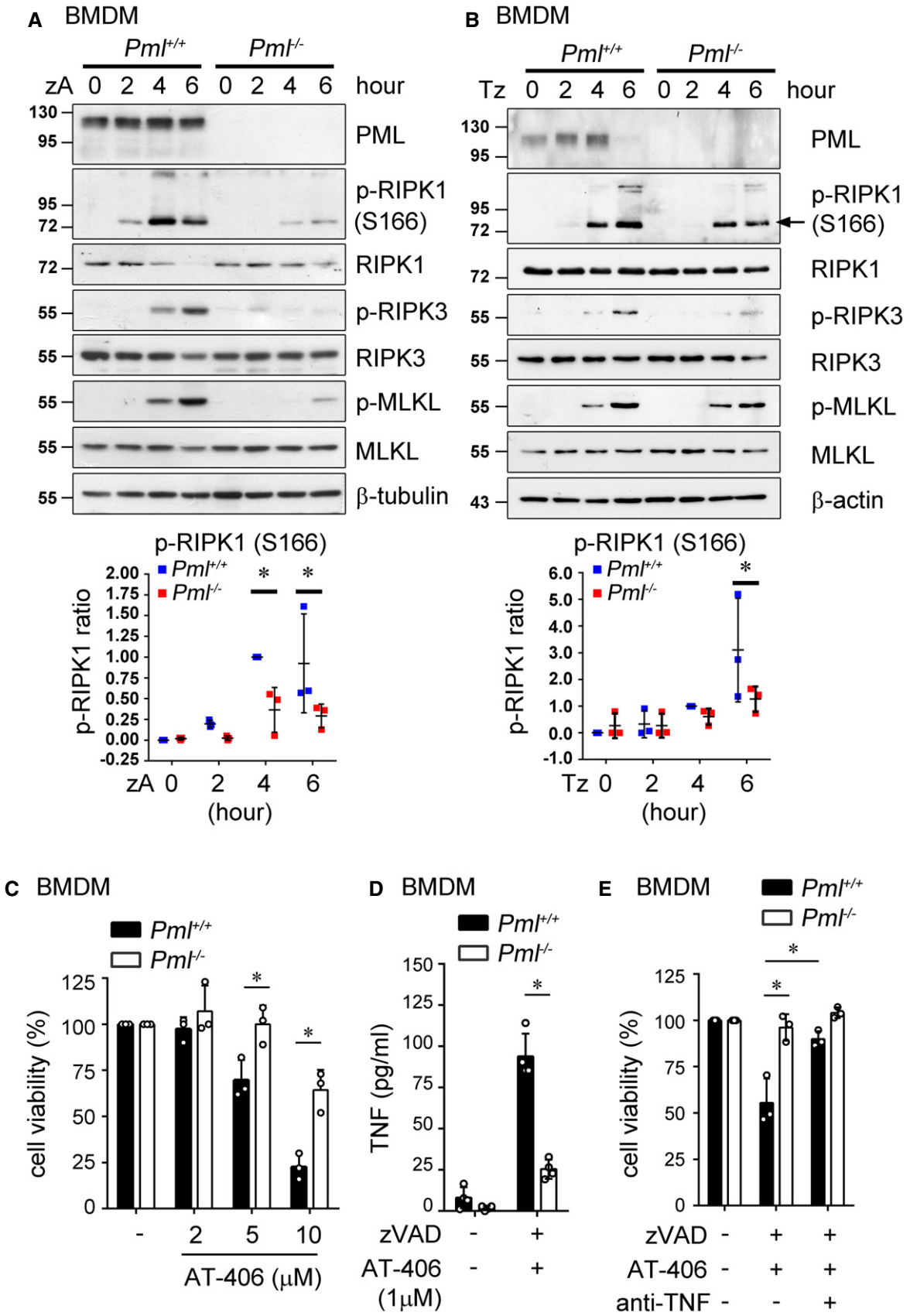
A BMDM
Pml+/+
Pml-/-
zA 0 2 4 6 0 2 4 6 hour
PML
p-RIPK1 (S166)
RIPK1
p-RIPK3
RIPK3
p-MLKL
MLKL
β-tubulin
B BMDM
Tz 0 2 4 6 0 2 4 6 hour
β-actin
p-RIPK1 (S166)
p-RIPK1 ratio
(hour)
C BMDM
cell viability (%)
AT-406 (μM)
D BMDM
TNF (pg/ml)
zVAD
AT-406 (1μM)
E BMDM
anti-TNF

Figure 2.

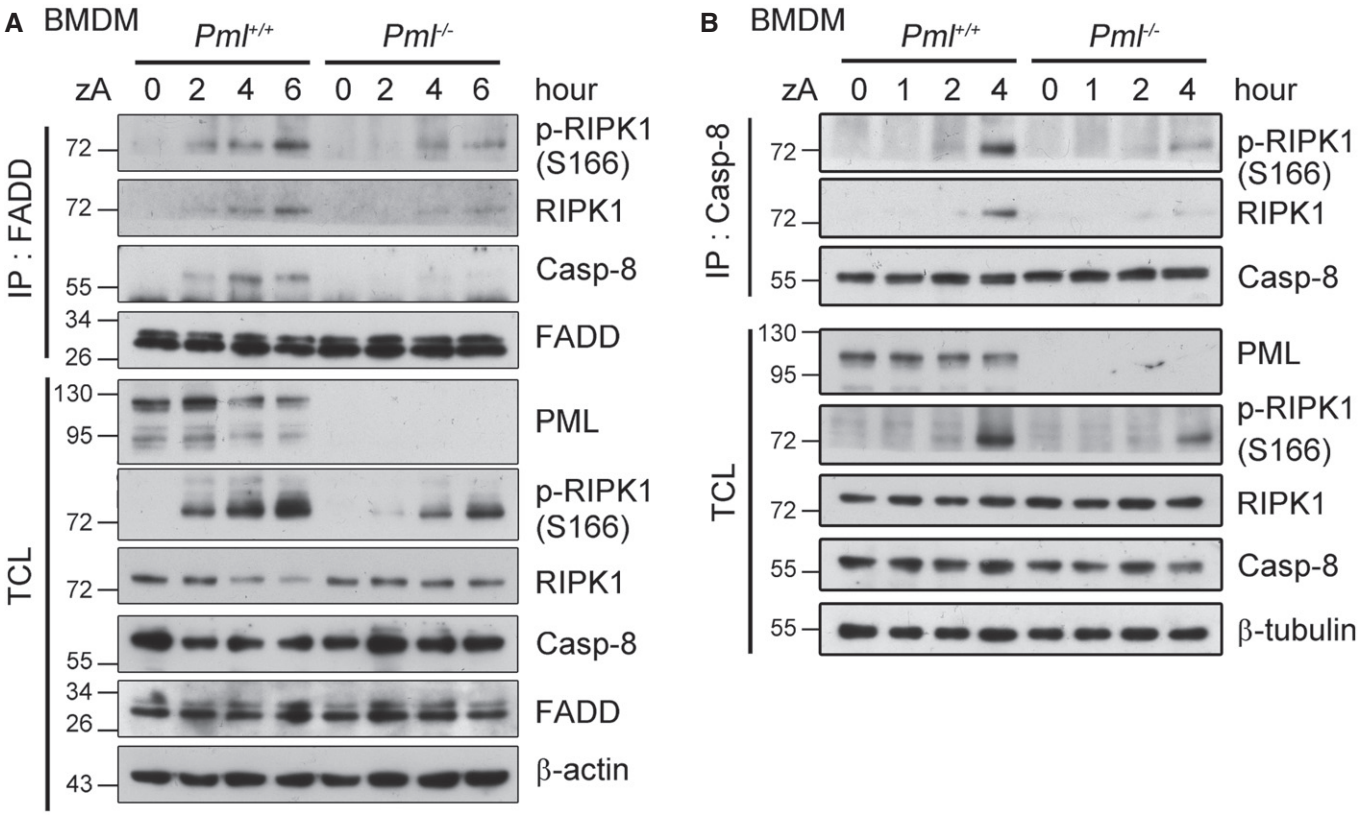

Figure 3. Diminished association of RIPK1 with FADD and caspase-8 in PML-deficient cells.

A *Pml*$^{+/+}$ and *Pml*$^{-/-}$ BMDMs were treated with zVAD for 30 min, followed by AT-406 (zA) treatment at the indicated time-points, before preparing total cell lysates (TCL). TCL were immunoprecipitated with anti-FADD, and the amounts of p-RIPK1[S166], RIPK1, and caspase-8 in the precipitates and TCL were analyzed.

B *Pml*$^{+/+}$ and *Pml*$^{-/-}$ BMDMs were treated with zVAD + AT-406 (zA) as in (A), and TCL were then harvested. TCL were immunoprecipitated with anti-caspase-8, and the contents of p-RIPK1[S166] and RIPK1 in the precipitates and TCL were analyzed.

Data information: Data (A, B) are representative of three biological replicates.
Source data are available online for this figure.

independently of IKKα/IKKβ-mediated NF-κB activation (Dondelinger *et al*, 2015). Following activation by p38 MAPK, MK2 directs RIPK1 S321/S326 phosphorylation, which inhibits the activation of RIPK1 kinase (marked by S166 autophosphorylation) and binding of RIPK1 with FADD/caspase-8 (Dondelinger *et al*, 2017; Jaco *et al*, 2017; Menon *et al*, 2017). We performed a detailed analysis of signaling in PML-deficient macrophages—including activations of IKKα/IKKβ, p38 MAPK, and MK2, as well as phosphorylation of RIPK1 at S321—after TNF + zVAD stimulation (Fig 5A and B). We observed that signaling was generally comparable between WT and *Pml*$^{-/-}$ BMDMs after treatment with TNF + zVAD (Fig 5A and B), with WT and *Pml*$^{-/-}$ BMDMs exhibiting similar extents of IKKα/IKKβ phosphorylation, IκBα degradation, ERK phosphorylation, and JNK phosphorylation (Fig 5A and B). In contrast, PML deficiency profoundly increased TNF + zVAD-mediated MK2 activation, with a prominent increase in MK2 phosphorylation in *Pml*$^{-/-}$ BMDMs that was associated with increased phosphorylation of RIPK1[S321] in *Pml*$^{-/-}$ BMDMs relative to WT controls (Fig 5A and B). That PML deficiency differentiates MK2-RIPK1 activation was even more prominent when BMDMs were stimulated with TNF alone (Fig EV1A–C). This outcome was attributable to enhanced activation of p38 MAPK in *Pml*$^{-/-}$ BMDMs (Fig EV1B and C), as reported previously (Shin *et al*, 2004), in the context of normal TNF-induced activation of TAK1 (which mediates MKK3-p38 MAPK activation) (Sato *et al*, 2005; Shim *et al*, 2005). The enhanced activation of MK2 and increased phosphorylation of RIPK1[S321] in *Pml*$^{-/-}$ BMDMs were also observed following zVAD + AT-406 stimulation (Fig EV1D). Furthermore, we detected increased MK2 phosphorylation and elevated RIPK1[S321] phosphorylation in *Pml*$^{-/-}$ MEFs stimulated with TNF + CHX (Fig EV1E).

Enhanced activation of p38 MAPK and MK2 could also be visualized in PML-deficient cells. By monitoring the appearance of activated p38 (phosphorylated p38, p-p38) MAPK in WT macrophages before and after TNF + zVAD treatment, we observed that p-p38 MAPK was practically absent from resting macrophages (Fig EV2A). TNF + zVAD stimulation resulted in an increase in p-p38 MAPK levels in the cytoplasm and nucleus of *Pml*$^{+/+}$ macrophages, which was further enhanced in *Pml*$^{-/-}$ macrophages (Fig EV2A and B) (Ben-Levy *et al*, 1998). The extent of MK2 activation was also correlated with PML deficiency. TNF + zVAD stimulation enhanced p-MK2 levels in WT macrophages, and PML deficiency greatly increased activated MK2 content in both the cytoplasm and nucleus

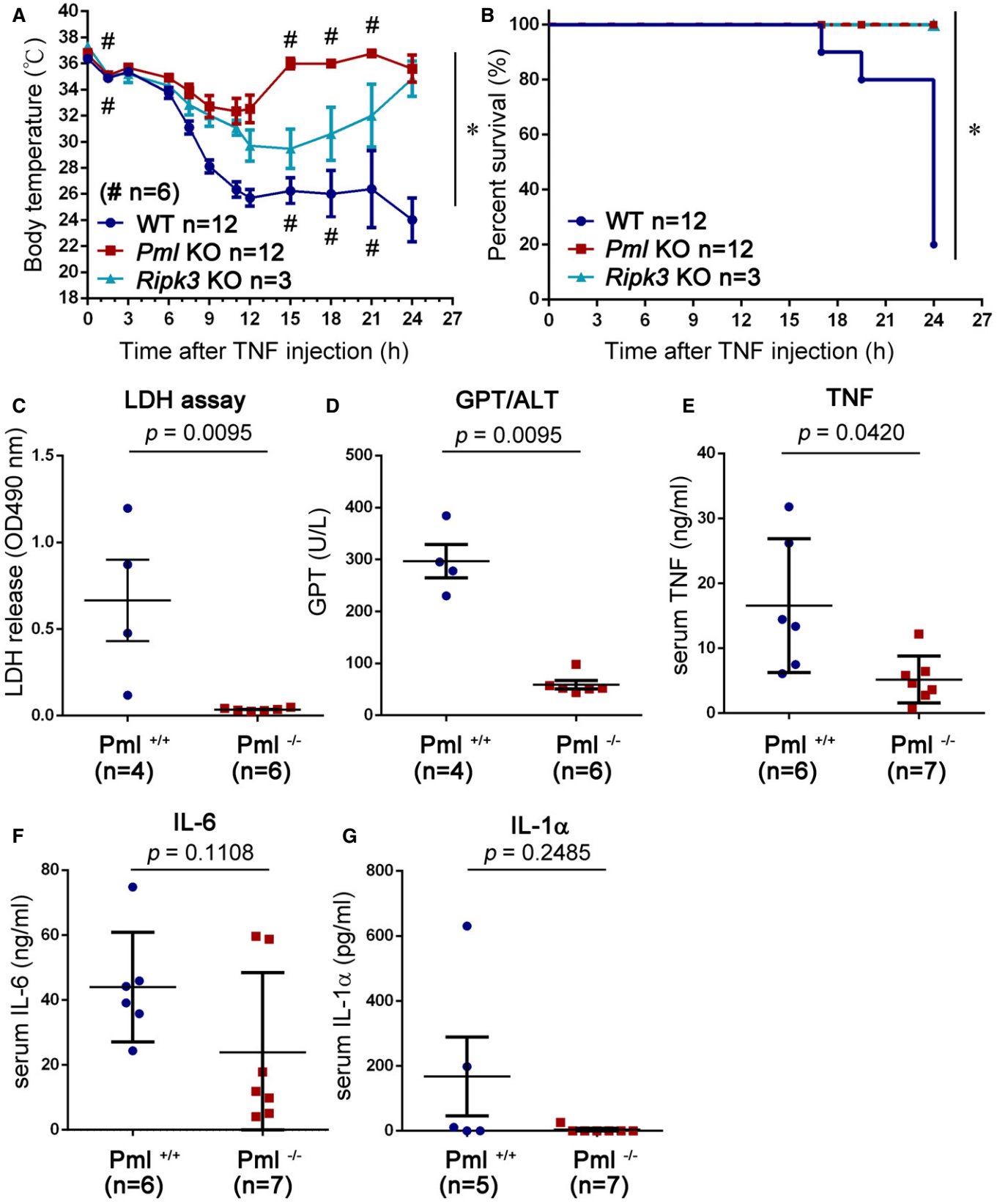

Figure 4.

Figure 4. Resistance to TNF-induced septic shock in *Pml*$^{-/-}$ mice.

A, B WT (*Pml*$^{+/+}$) and *Pml*$^{-/-}$ mice (n = 12 in each group) and *Ripk3*$^{-/-}$ mice (n = 3) were injected with mouse TNF (1.5 μg/g body weight), and rectal body temperature (A) and survival (B) were determined at the indicated time-points. #, the temperature of only six mice was measured at the indicated time-points. Mean ± SEM is shown. *P < 0.05 as determined by two-way ANOVA (A), or by log-rank (Mantel–Cox) test (B).

C, D WT and *Pml*$^{-/-}$ mice were injected with TNF, and serum samples from live mice were collected 30 h later. Levels of LDH (C) and GPT/ALT (D) were quantitated. Mean ± SEM is shown. P = 0.0095 (C, D) by unpaired t-test with Welch's correction.

E–G Serum levels of TNF (E), IL-6 (F), and IL-1α (G) from WT and *Pml*$^{-/-}$ mice 12 h after TNF injection. Mean ± SEM is shown. Indicated P-values were calculated using unpaired t-test with Welch's correction.

Source data are available online for this figure.

of *Pml*$^{-/-}$ macrophages (Fig EV2C and D). Therefore, PML deficiency leads to increased activation of p38 MAPK and MK2, which can be clearly visualized in cells.

We noted a decrease in IKKα/IKKβ phosphorylation in *Pml*$^{-/-}$ BMDMs, accompanied by diminished IκBα phosphorylation, indicative of reduced activation of IKK and NF-κB in *Pml*$^{-/-}$ BMDMs stimulated by TNF alone (Fig EV1A), even though the effect was less obvious when *Pml*$^{-/-}$ BMDMs were treated with TNF + zVAD (Fig 5A). Attenuated NF-κB activation could also be observed in *Pml*$^{-/-}$ MEFs treated with TNF + CHX (Fig EV1F). Therefore, this reduction in NF-κB activation, which presumably would lead to increased apoptosis, is not associated with the decrease in necroptosis displayed by PML-deficient cells. In terms of noncanonical NF-κB activation, PML-knockout did not apparently affect the appearance of NF-κB-inducing kinase (Cai *et al* 2011) or p52 upon zVAD + AT-406 treatment (Fig EV1G).

We also examined the role of MK2-mediated RIPK1 phosphorylation in the protection against necroptosis mediated by PML deficiency. To do so, we generated RIPK1-knockout and RIPK1-PML-double knockout MEFs (Appendix Fig S4A). RIPK1 knockout eliminated the sensitivity of WT MEFs to the necroptosis induced by TNF + zVAD (Appendix Fig S4B). Reintroduction of WT RIPK1 to *Ripk1*$^{-/-}$ MEFs sensitized them to the necroptosis triggered by TNF + zVAD, whereas re-expression of WT RIPK1 in *Pml*$^{-/-}$*Ripk1*$^{-/-}$ MEFs rendered them partially resistant to necroptosis (Appendix Fig S4C and D). In contrast, introduction of RIPK1[S336A] into *Pml*$^{-/-}$*Ripk1*$^{-/-}$ MEFs increased both spontaneous and TNF + zVAD-induced necroptosis (Appendix Fig S4C and E), suggesting that the protective effect of PML deficiency is at least partially associated with RIPK1[S336] phosphorylation.

MK2 inhibitor or MK2 knockout eliminates the protective effect of PML deficiency

We also employed an MK2 inhibitor to examine the association between MK2 and necroptosis. The efficacy of the MK2 inhibitor PF-3644022 was demonstrated by the profound death observed after treating WT and *Pml*$^{-/-}$ BMDMs with TNF + zVAD + PF-3644022, indicating complete elimination of the protective effect of PML deficiency (Fig EV3A). The presence of this MK2 inhibitor enhanced pro-necroptotic phosphorylation of RIPK1[S166] and MLKL in WT and *Pml*$^{-/-}$ BMDMs stimulated with either TNF + zVAD or zVAD + AT-406 (Fig EV3B and C). PML deficiency-associated attenuation in p-RIPK1[S166] and p-MLKL was completely reversed by MK2 inhibitor treatment during necroptosis induction (Fig EV3B and C). Moreover, even though PF-3644022 alone only triggered a small degree of hypothermia without death, administration of PF-3644022 increased the susceptibility of WT mice to TNF-induced hypothermia and death (Fig 5C and D), as previously documented (Dondelinger *et al*, 2017). The MK2 inhibitor also eliminated the protective effect of PML deficiency in terms of TNF-induced septic shock, with PF-3644022-treated *Pml*$^{-/-}$ mice becoming sensitive to TNF-triggered hypothermia and death (Fig 5E and F).

We also generated *Mk2*$^{-/-}$ mice to examine the specific role of MK2 in PML-regulated necroptosis. MK2 knockout did not affect the p38 MAPK activation stimulated by TNF + zVAD (Fig 6A). The phosphorylation of RIPK1[S321] induced by TNF + zVAD or zVAD + AT-406 was completely abrogated by MK2 knockout (Fig 6A and B). Consequently, MK2 knockout greatly sensitized WT macrophages to necroptosis induction (Fig EV3D). The enhanced necroptosis displayed by *Mk2*$^{-/-}$ BMDMs could be partially attributed to increased autocrine TNF production upon zVAD + AT-406 treatment, relative to WT controls (Fig EV3E). MK2 knockout also eliminated the protective effect of PML deficiency against necroptosis triggered by TNF + zVAD or zVAD + AT-406 (Fig 6C and D). The MLKL phosphorylation induced by zVAD + AT-406, which was almost completely abrogated by PML knockout, became prominent with additional MK2 knockout (Fig 6E). The critical role of MK2 in the protective effect of PML deficiency was further confirmed by assessment of TNF-induced septic shock. MK2 knockout sensitized WT mice to TNF-triggered death and hypothermia, it completely eliminated the resistance of *Pml*$^{-/-}$ mice to TNF treatment (Fig 6F and G), and it was accompanied by elevated seral levels of LDH 3 h after TNF administration (Fig 6H). Therefore, the PML deficiency

Figure 5. PML deficiency enhances phosphorylation of p38 MAPK, MK2, and RIPK1[S321], and a MK2 inhibitor restores necroptosis.

A *Pml*$^{+/+}$ and *Pml*$^{-/-}$ BMDMs were treated with TNF (100 ng/ml) + zVAD (20 μM) for the indicated timeframes. The contents of p-IKKα/β, IKKα/β, IκBα, p-MK2, and MK2 were analyzed by immunoblotting.

B *Pml*$^{+/+}$and *Pml*$^{-/-}$ BMDMs were treated with TNF (100 ng/ml) + zVAD (20 μM) for the indicated times, and levels of p-RIPK1[S321], RIPK1, p-JNK, JNK, p-ERK, ERK, p-p38, and p38 at the indicated time-points were then determined.

C–F WT (*Pml*$^{+/+}$) and *Pml*$^{-/-}$ mice were treated with DMSO or Nec-1s (6 μg/g) or MK2 inhibitor PF-3644022 (75 μg/mouse) by intraperitoneal injection 15 min before and 60 min after intravenous TNF (1.5 μg/g body weight) injection. Body temperature (C, E) and survival (D, F) were monitored. Experiments C-F were conducted concurrently. Mean ± SEM is shown (C, E). P-values were determined by two-way ANOVA for multiple comparisons (C, E) or by log-rank (Mantel–Cox) test (D, F).

Source data are available online for this figure.

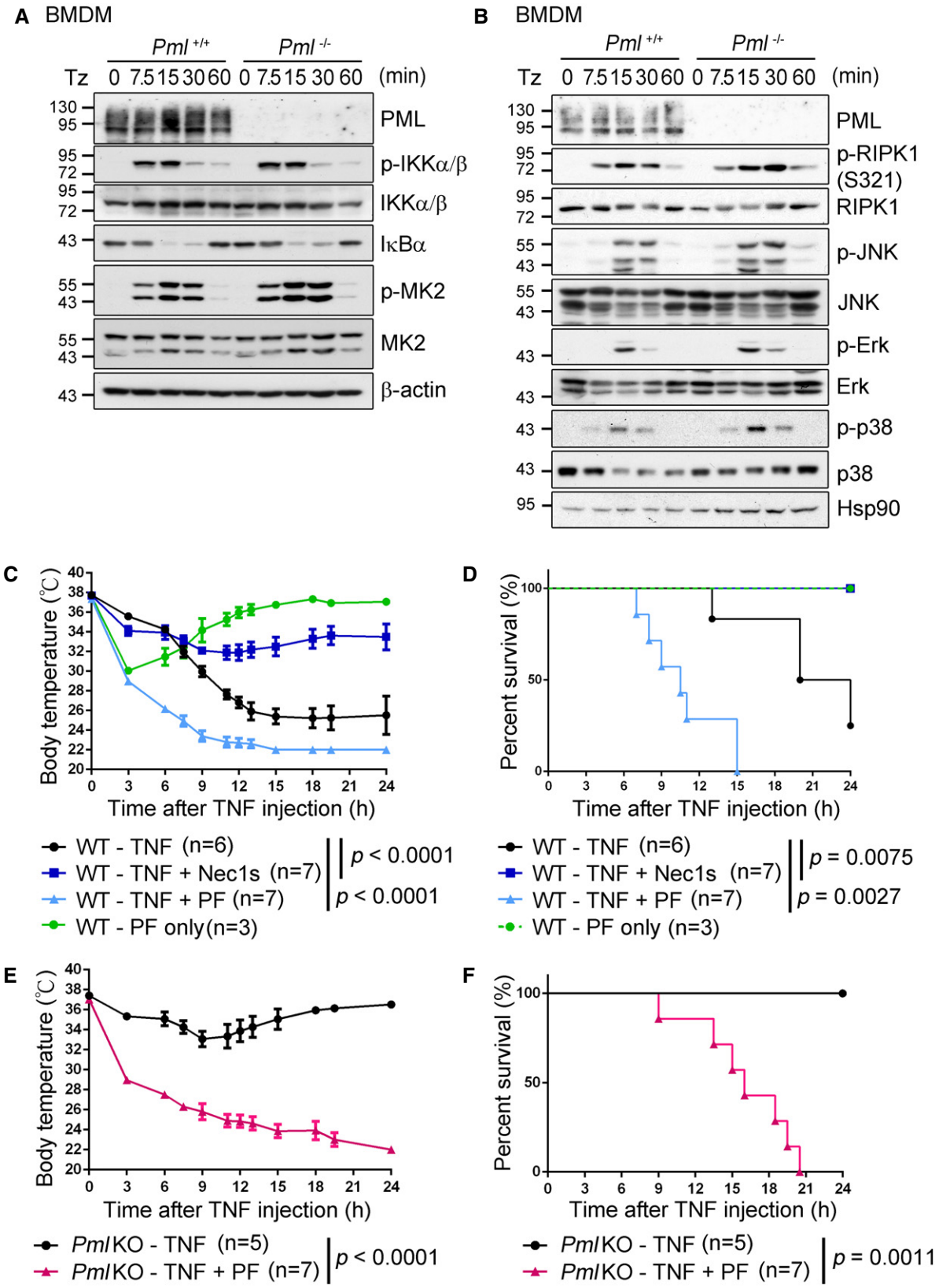
A BMDM
Pml +/+
Pml -/-
Tz 0 7.5 15 30 60 0 7.5 15 30 60 (min)
PML
p-IKKα/β
IKKα/β
IκBα
p-MK2
MK2
β-actin
B BMDM
Pml +/+
Pml -/-
Tz 0 7.5 15 30 60 0 7.5 15 30 60 (min)
PML
p-RIPK1 (S321)
RIPK1
p-JNK
JNK
p-Erk
Erk
p-p38
p38
Hsp90
C
Body temperature (℃)
Time after TNF injection (h)
WT - TNF (n=6)
WT - TNF + Nec1s (n=7)
WT - TNF + PF (n=7)
WT - PF only(n=3)
p < 0.0001
p < 0.0001
D
Percent survival (%)
Time after TNF injection (h)
WT - TNF (n=6)
WT - TNF + Nec1s (n=7)
WT - TNF + PF (n=7)
WT - PF only (n=3)
p = 0.0075
p = 0.0027
E
Body temperature (℃)
Time after TNF injection (h)
PmlKO - TNF (n=5)
PmlKO - TNF + PF (n=7)
p < 0.0001
F
Percent survival (%)
Time after TNF injection (h)
PmlKO - TNF (n=5)
PmlKO - TNF + PF (n=7)
p = 0.0011

Figure 5.

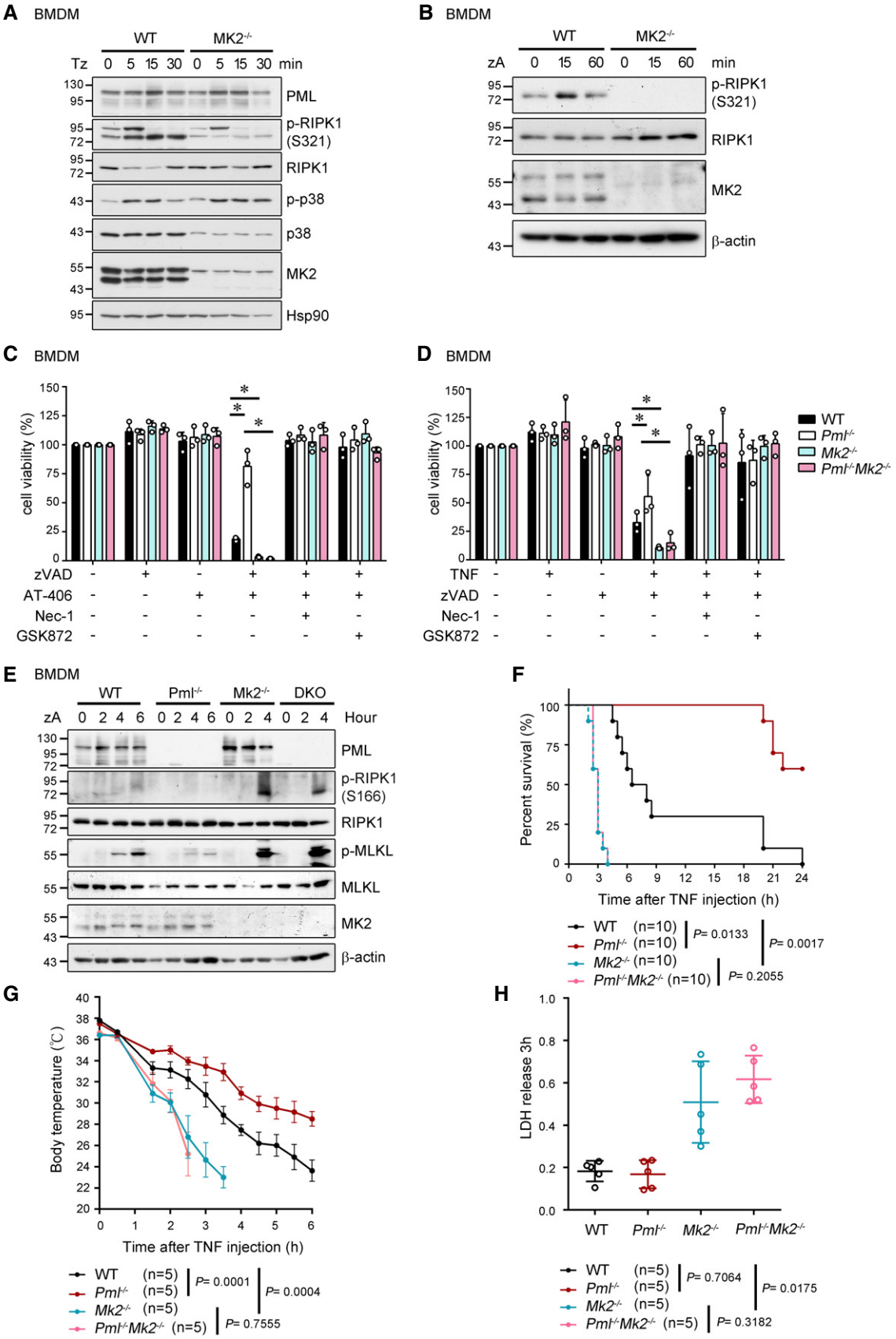

Figure 6.

Figure 6. MK2 deficiency confers sensitivity of PML-null cells to necroptosis.

A, B WT and *Mk2*$^{-/-}$ BMDMs were treated with TNF (100 ng/ml) + zVAD (20 μM) (A) or with zVAD (20 μM) + AT-406 (1 μM) (B), and then, the contents of p-RIPK1 [S321], RIPK1, p-p38, and p38 were determined at the indicated time-points.

C WT, *Pml*$^{-/-}$, *Mk2*$^{-/-}$, and *Pml*$^{-/-}$*Mk2* $^{-/-}$ BMDMs were treated with zVAD (20 μM), AT-406 (1 μM), Nec-1 (40 μM), and GSK872 (10 μM), as indicated, for 18 h. Cell viability was determined by ATP release. Data show mean ± SD of three biological replicates. *$P < 0.05$ for multiple *t*-tests according to the Holm–Sidak method.

D WT, *Pml*$^{-/-}$, *Mk2*$^{-/-}$, and *Pml*$^{-/-}$*Mk2* $^{-/-}$ BMDMs were treated with TNF (100 ng/ml), zVAD (20 μM), Nec-1 (40 μM), and GSK872 (10 μM), as indicated, for 16 h. Cell viability was determined by ATP release. Data show mean ± SD of three biological replicates. *$P < 0.05$ for multiple *t*-tests according to the Holm–Sidak method.

E WT, *Pml*$^{-/-}$, *Mk2*$^{-/-}$, and *Pml*$^{-/-}$*Mk2* $^{-/-}$ BMDMs were treated with zVAD (20 μM) and AT-406 (1 μM) for the indicated timeframes. The levels of RIPK1, p-RIPK1 [S166], RIPK3, p-RIPK3, MLKL, and p-MLKL in cell lysates were analyzed by immunoblots. Results are representative of three biological replicates.

F WT, *Pml*$^{-/-}$, *Mk2*$^{-/-}$, and *Pml*$^{-/-}$*Mk2* $^{-/-}$ mice were injected i.v. with TNF (1.5 mg/kg), and survival was monitored for 24 h. Data represent a combination of two independent experiments ($n = 10$). *$P < 0.05$ for log-rank (Mantel–Cox) test.

G, H WT, *Pml*$^{-/-}$, *Mk2*$^{-/-}$, and *Pml*$^{-/-}$*Mk2* $^{-/-}$ mice ($n = 5$) were injected i.v. with TNF (1.5 mg/kg), before recording body temperature for the next 6 h (G), and collecting serum samples at 3 h to quantitate LDH release (H). *$P < 0.05$ as determined by two-way ANOVA (G), or *P*-values calculated by unpaired *t*-test with Welch's correction (H).

Source data are available online for this figure.

that confers resistance to necroptosis and apoptosis is abrogated by MK2 inhibition or MK2 knockout, so the protective effect of necroptosis in PML-knockout cells and mice could be largely attributable to enhanced MK2 activation.

PML inhibits p38-MK2 association

We investigated how activation of p38 MAPK and MK2 could be inhibited by PML. We identified MK2 as a new interaction partner of PML. Overexpressed PML-I interacted with MK2 in HEK293T cells (Fig EV4A). Co-expression of MK2 with PML-I resulted in preferential co-localization of MK2 with PML NBs (Fig EV4B). The N-terminal fragment of MK2 was primarily responsible for mediating the interaction with PML (Fig EV4C), and it was the N-terminal part of PML (exon 1–4) that bound MK2 (Fig EV4D). Furthermore, interaction between endogenous PML and MK2 was revealed by their co-precipitation in macrophages stimulated with TNF + zVAD (Fig 7A). In addition, proximal association of MK2 with PML NBs was apparent in macrophages before and after TNF stimulation (Fig EV4E).

The interaction between PML and p38 MAPK was reported in a previous study showing that PML binds to p38 MAPK and suppresses its activation (Shin *et al*, 2004). We found that overexpressed p38 MAPK co-precipitated with PML-I or PML-IΔNLS in HEK293T cells (Fig EV5A). Consistent with a previous finding that the C-terminal part of PML binds p38 (Shin *et al*, 2004), we found that the interaction between exons 1-4 of PML-I and p38 was very weak, relative to WT PML-I (Fig EV5A). Consequently, overexpression of WT PML-I increased the sensitivity of primary MEFs to necroptosis induction, an effect that was attenuated when instead we overexpressed PML-I exons 1-4 (Fig EV5B). For endogenous PML and p38 MAPK, immunoprecipitation of p38 MAPK from resting macrophages pulled down a very small amount of PML, with the association of PML-p38 MAPK only becoming prominent after macrophages were stimulated with TNF (Fig 7B). Similarly, p38 and its upstream kinase MKK3 were pulled down by PML in BMDMs upon treatment with TNF + zVAD (Fig 7C). Enhanced interaction between PML and p38 MAPK was also observed in MEFs treated with TNF + BMS-345541 to induce apoptosis (Fig EV5C). Similarly, p38 MAPK co-localization with PML NBs in resting macrophages significantly increased upon TNF stimulation, a trend also observed for p-p38 (Fig EV5D). Therefore, TNF stimulation strengthened the typically weak interaction between PML and p38.

We then examined how PML affects the interaction between MK2 and p38 MAPK. PML overexpression inhibited binding between p38 MAPK and MK2 in HEK293T cells (Fig EV5E). Immunoprecipitation of p38 MAPK in BMDMs revealed that p38 is constitutively associated with MK2 (Fig 7D), and PML deficiency modestly increased the association between p38 MAPK and MK2 in macrophages before and after TNF + zVAD stimulation. This outcome was followed by a clear reduction in p38-MK2 association in *Pml*$^{-/-}$ BMDMs at 30 min (Fig 7D), suggesting that MK2 dissociates from p38 MAPK to target downstream substrates upon activation by p38 MAPK (Ben-Levy *et al*, 1998; Engel *et al*, 1998). Image analysis confirmed that PML deficiency enhanced co-localization of MK2 and p38 MAPK in macrophages before and after TNF activation (Fig EV5F–H). Direct competition between PML and p38 for MK2 was further demonstrated by increasing amounts of PML protein reducing the binding between recombinant MK2 and p38 *in vitro* (Fig 7E). Moderate activation of recombinant MK2 protein, likely by kinase dimerization, was enhanced by the presence of p38 protein, and it was suppressed by recombinant PML protein (Fig 7F). Therefore, PML inhibits MK2-p38 MAPK association, thereby reducing activation of MK2 by p38 MAPK.

Figure 8 summarizes our findings, suggesting that PML targets activation of the p38-MK2-RIPK1 cascade. PML suppresses activation of MK2 by interfering with binding of p38 MAPK to MK2, an essential step in MK2 activation. PML deficiency enhanced the activation of MK2 and phosphorylation of RIPK1[S321], and it also attenuated necroptosis. Inhibition or deletion of MK2 eliminated RIPK1[S321] phosphorylation and the protective effect of PML deficiency against necroptosis. For necroptosis initiated by a SMAC mimetic, PML is required for autocrine production of TNF. PML deficiency reduces autocrine TNF secretion and associated necroptosis induction, exhibiting a differential process of protecting against necroptosis. Overall then, PML may contribute to TNF-induced necroptosis via two distinct pathways, firstly by inhibiting MK2 activation and secondly by promoting autocrine TNF generation.

Discussion

In the present study, we illustrate how PML is involved in necroptosis. The absence of PML resulted in resistance to TNF-induced necroptosis (Fig 1, Appendix Fig S1). The diminished necroptosis in

these PML-deficient cells was associated with reduced phosphorylation of RIPK1[S166], RIPK3, and MLKL (Fig 2, Appendix Fig S3), as well as attenuated formation of the FADD-caspase-8-RIPK1-RIPK3 necroptotic complex (Fig 3, Appendix Fig S3). PML deficiency also inhibited RIPK1-mediated apoptosis (Fig 1E, Appendix Fig S2A) and RIPK1-independent apoptosis (Appendix Fig S2B). Thus, PML-knockout mice were protected from TNF-induced systemic inflammatory response syndrome, which is mediated by necroptosis and apoptosis (Fig 4). These results unveil a previously unknown role of PML in suppressing TNF-induced necroptosis.

PML targets the necroptotic pathway at the stage of RIPK1, with PML suppressing MK2-mediated phosphorylation of RIPK1[S321] (Fig 5). PML deficiency led to attenuated RIPK1 kinase activation (represented by S166 phosphorylation) (Figs 2A and B, and 3A and B, Appendix Fig S3A and C), accompanied by enhanced p38 MAPK activation, increased MK2 activation, and elevated RIPK1[S321] phosphorylation (Figs 5A and B, EV1A–F and EV2A–D). Therefore, reduced formation of the FADD-caspase-8-RIPK1-RIPK3 complex (Fig 3, Appendix Fig S3D) is attributable to increased phosphorylation of RIPK1 at S321 by MK2 in PML-deficient cells.

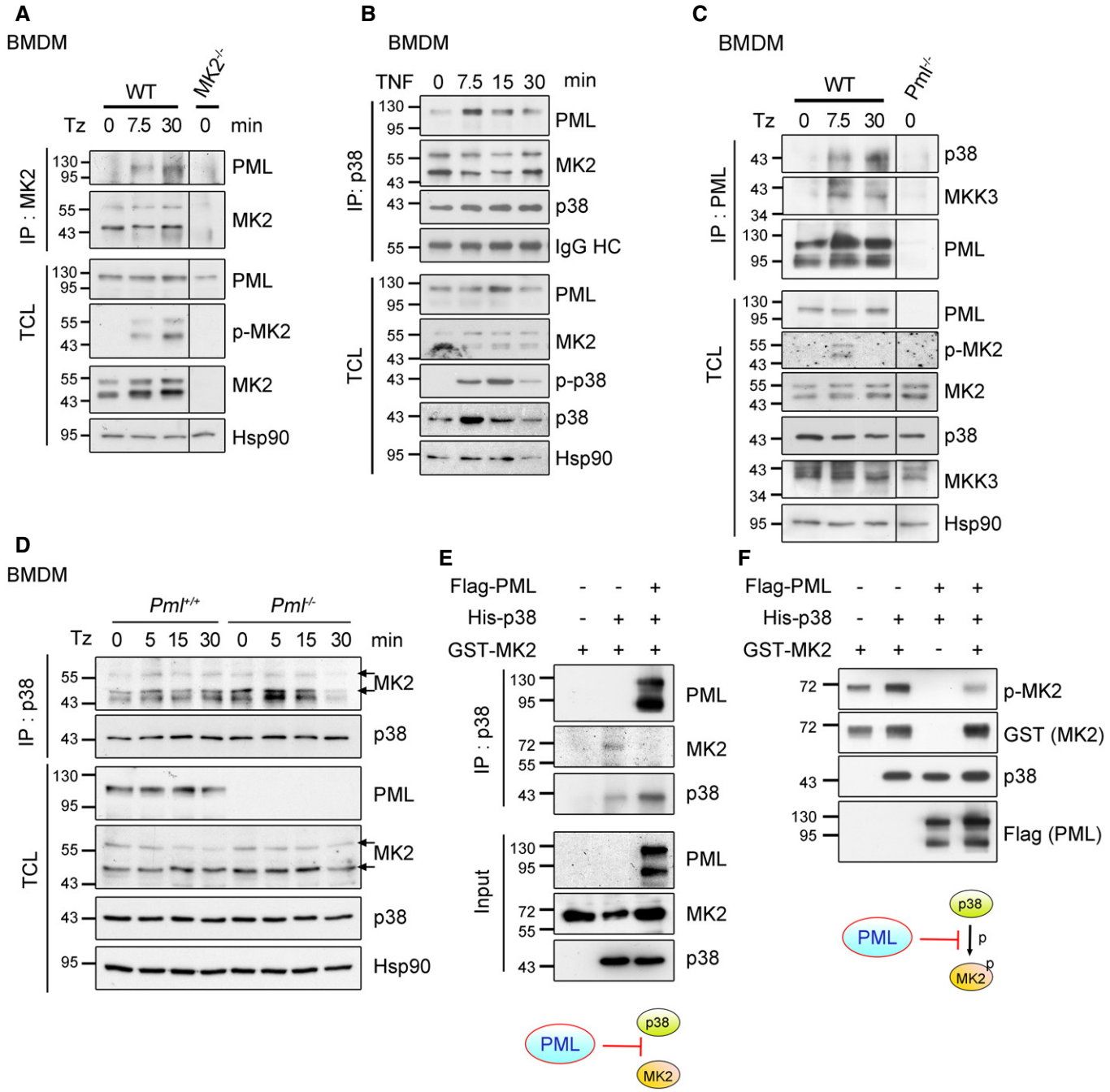

Figure 7.

Figure 7. PML interacts with MK2 and inhibits p38 MAPK-MK2 association.

A WT BMDMs were treated with TNF (100 ng/ml) + zVAD (20 μM) for the indicated times. Cell lysates were immunoprecipitated with anti-MK2, and levels of PML were determined. *Mk2*$^{-/-}$ BMDMs served as a negative control.

B WT BMDMs were treated with TNF (100 ng/ml) for the indicated times, before immunoprecipitating p38 MAPK and determining the levels of PML, p38, and MK2 in the precipitates and total cell lysates.

C WT BMDMs were treated with TNF (100 ng/ml) + zVAD (20 μM) for the indicated times. Cell lysates were immunoprecipitated with anti-PML, and levels of p38 and MKK3 were determined. *Pml*$^{-/-}$ BMDMs served as a negative control.

D WT and *Pml*$^{-/-}$ BMDMs were treated with TNF (100 ng/ml) + zVAD (20 μM) for the indicated times. p38 MAPK was immunoprecipitated, and its association with MK2 was then analyzed.

E Recombinant Flag-PML-I, GST-MK2 (60 ng), and His-p38 (60 ng) were incubated, as indicated, at 4°C for 2 h. p38 was pulled down by anti-p38, and then, PML, MK2, and p38 contents in the precipitate and reaction mixture (input) were detected by immunoblotting.

F Recombinant Flag-PML-I, GST-MK2 (100 ng), and His-p38 (200 ng) were incubated, as indicated, at 30°C in *in vitro* kinase assay buffer (20 mM HEPES, 10 mM $MgCl_2$, 100 nM ATP, 1 mM DTT) for 20 min. The levels of p-MK2, MK2, p38, and PML (FLAG) in the reaction mixture were then determined.

Data information: Experiments (A–F) were independently repeated three times (biological replicates) and generated similar results.
Source data are available online for this figure.

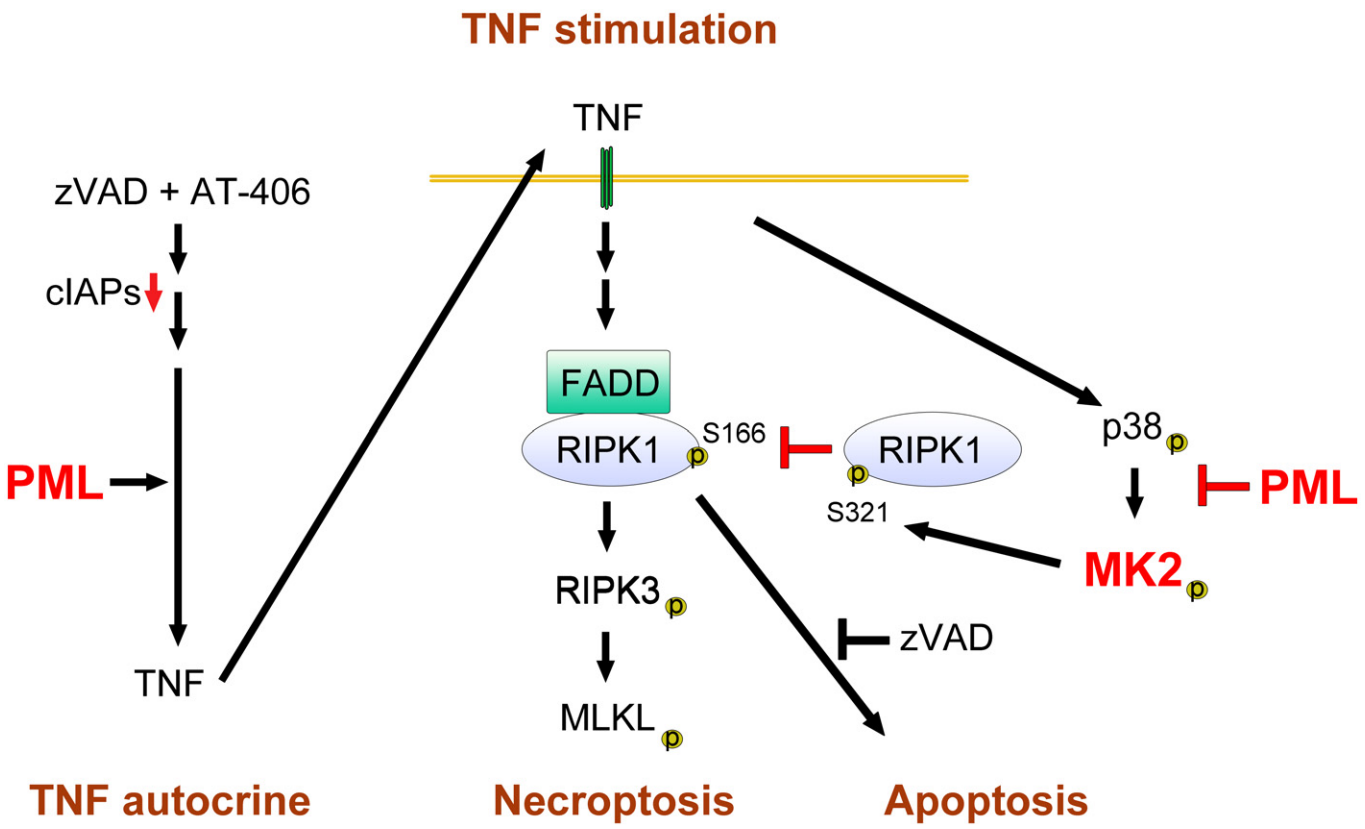

Figure 8. Model depicting how PML promotes necroptosis.

PML exhibits two different mechanisms to promote necroptosis. In PML-sufficient cells, PML binds p38 MAPK and MK2 and attenuates p38-mediated MK2 activation. The reduction in MK2-directed RIPK1[S321] phosphorylation enables RIPK1 activation, represented by RIPK1[S166] phosphorylation, and RIPK1-RIPK3-MLKL necroptotic complex formation. In PML-deficient cells, increased MKK3-p38-MK2 activation leads to enhanced RIPK1[S321] phosphorylation, which suppresses RIPK1 activation and necroptosis. For necroptosis induced by a SMAC mimetic (such as AT-406) plus zVAD, PML promotes autocrine TNF production, leading to enhanced necroptosis. PML deficiency reduces SMAC mimetic-induced autocrine TNF generation and limits the associated necroptosis.

Notably, the impact of PML deficiency was more prominent when macrophages were treated with zVAD + AT-406 than with TNF + zVAD. As previously documented (Varfolomeev *et al*, 2007; Vince *et al*, 2007), we found that autocrine TNF was induced by zVAD + AT-406 and that neutralization of TNF blocked necroptosis in WT macrophages (Fig 2D and E), confirming the death-initiating role of TNF. Moreover, PML knockout inhibited SMAC mimetic-induced TNF production (Fig 2D). Therefore, while PML deficiency enhances MK2 activation and RIPK1[S321] phosphorylation to antagonize the necroptosis initiated by TNF + zVAD, it also eliminates the availability of TNF for the necroptosis triggered by zVAD + AT-406, providing an additional level of protection.

Many PML-directed biological activities are associated with PML-interacting proteins. More than 150 proteins have been found to bind PML either constitutively or transiently (Mohamad & Boden, 2010). PML interacts with transcription factors including p53, c-Fos, Nur77, RelA, and Myc, with c-Jun acting as a co-factor for these transcription factors (Zhong *et al*, 2000; Wu *et al*, 2002). PML also regulates transcriptional activation by recruiting CREB-binding protein (CBP) or histone deacetylase (HDAC) to nuclear bodies (Doucas *et al*, 1999; Wu *et al*, 2001). Moreover, PML can regulate biological functions by sequestering proteins within the nucleus. Interaction with and sequestration of Daxx by PML relieves Daxx-directed transcriptional repression, leading to transcriptional activation of glucocorticoid receptor (Li *et al*, 2000; Lin *et al*, 2003). PML also enhances p53 stability by sequestering MDM2 in the nucleolus and promoting p53-induced transcription (Bernardi *et al*, 2004). Conversely, p53 is destabilized by Mad1 via interference with PML-directed sequestration of MDM2 (Wan *et al*, 2019), illustrating that PML-mediated physiological functions can be regulated by modulating the sequestering ability of PML.

PML is known to interact with p38 and inhibit p38 activation (Shin *et al*, 2004). In the present study, we have further identified a previously unappreciated function of PML through its interaction with MK2 (Figs 7A and EV4). Activation of MK2 and p38 MAPK takes place in the nucleus, followed by translocation of active p38 MAPK and MK2 into the cytoplasm (Ben-Levy *et al*, 1998; Engel *et al*, 1998; Shin *et al*, 2004). We observed that PML bound both MK2 and p38 MAPK and inhibited the interaction between p38 MAPK and MK2. Increasing amounts of PML inhibited p38 MAPK-MK2 association *in vivo* (Fig EV5E), whereas PML deficiency promoted endogenous p38 MAPK-MK2 binding (Fig EV5F–H). In our *in vitro* system consisting only of recombinant PML, p38 MAPK, and MK2 proteins, PML inhibited p38 MAPK-MK2 interaction and suppressed MK2 activation (Fig 7E and F). Therefore, PML inhibits activation of MK2 in part by interfering with the critical step of p38 MAPK binding to MK2. Our finding that PML inhibits p38/MK2 to promote necroptosis supports a previous study showing that a p38/MK2 inhibitor enhances SMAC mimetic-induced necroptosis (Lalaoui *et al*, 2016).

In contrast to MK2, the effect of PML in NF-κB activation is less straightforward. A previous study indicated that PML interacts with RelA/p65 and inhibits NF-κB activation (Wu *et al*, 2003). Another study demonstrated that PML does not affect IκB degradation or p65 nuclear translocation, but it is required for transcription activity of NF-κB (Ahmed *et al*, 2017). The discrepancy between those studies could be due to differences in the cell types used. In the current study, we found that NF-κB activation induced by TNF or TNF + CHX was attenuated in *Pml*$^{-/-}$ BMDMs (Fig EV1A and F), but activation was comparable when WT and *Pml*$^{-/-}$ BMDMs were treated with TNF + zVAD (Fig 5A). We also found that noncanonical NF-κB activation, marked by levels of NIK and p52, was not affected by PML deficiency in *Pml*$^{-/-}$ BMDMs treated with zVAD + AT-406 (Fig EV1G). Therefore, as yet, we have not identified exactly how PML promotes the autocrine TNF expression that contributes to necroptosis triggered by the SMAC mimetic. Further works will be required to determine the involvement of PML in TNF autocrine production.

PML is a tumor suppressor that exhibits a variety of anti-cancer functions. It promotes mitochondrial respiration and increases the chemo-sensitivity of ovarian cancer (Gentric *et al*, 2019), and it maintains tumor microenvironments that are immunocompetent, and prevents metastases (Wang *et al*, 2017b). One of the best-known tumor-suppressing activities of PML is linked to its capacity to induce apoptotic cell death (Bernardi *et al*, 2008) and enhance TNF-triggered apoptotic death (Wu *et al*, 2003). In this study, we have also demonstrated a contribution of PML to TNF-triggered apoptosis (Fig 1E, Appendix Fig S2A–C). We have previously shown that PML also participates in NLRP3 inflammasome activation (Lo *et al*, 2013), leading to pyroptotic death. Thus, given our findings relating to necroptosis in the present study, PML has now been shown to promote cell death in the form of apoptosis, pyroptosis, and necroptosis. Notably, both apoptosis and necroptosis are involved in TNF-induced systemic inflammatory response syndromes (SIRS) (Newton *et al*, 2016), with the protective effect of PML deficiency against SIRS (Fig 4) confirming the *in vivo* role of PML in apoptosis and necroptosis.

Necroptosis is initiated under conditions by which FADD-caspase-8 apoptotic processes are blocked, serving as an alternative cell death pathway to apoptosis. Therefore, necroptosis plays a prominent role in triggering cancer cell death and suppressing tumors (Su *et al*, 2016; Galluzzi *et al*, 2017; Wang *et al*, 2017a). This role is also demonstrated by the way different cancers down-regulate RIPK1, RIPK3, and MLKL (Nugues *et al*, 2014; Feng *et al*, 2015; Koo *et al*, 2015; Lalaoui & Brumatti, 2017), which acts as a mechanism by which tumor cells can escape necroptosis (Galluzzi *et al*, 2017; Najafov *et al*, 2017). The use of SMAC mimetics is one approach to inducing necroptosis in cancer cells (He *et al*, 2009). Moreover, necroptosis elicits inflammation that enhances the priming of anti-cancer immunity (Kearney & Martin, 2017; Krysko *et al*, 2017; Lalaoui & Brumatti, 2017). Given that MK2 kinase phosphorylates RIPK1[S321], our observations that an MK2 inhibitor or MK2 knockout abrogated resistance to necroptosis in PML-deficient mice (Figs 5E and F, 6C–G and EV3) reveal a pivotal role for MK2 in PML activity. Thus, our finding that MK2 is inhibited by PML implies a promising avenue for targeting the tumor-suppressing functions of PML.

MK2 has been implicated as having a tumorigenic role in intestinal, colorectal, skin, bladder, and prostate cancers (Menon & Gaestel, 2018). MK2 in intestinal mesenchymal cells promotes colitis-associated carcinogenesis by enhancing epithelial proliferation and angiogenesis, while also inhibiting apoptosis (Henriques *et al*, 2018). Moreover, MK2 contributes to colon tumor progression by promoting polarization of tumor-associated macrophages into M2-like macrophages that are pro-tumorigenic and pro-angiogenic (Suarez-Lopez *et al*, 2018). Thus, direct inhibition of the MK2 activation cascade constitutes a previously unknown tumor-suppressing role for PML. In addition, the p38-MK2 axis participates in inflammatory diseases such as rheumatoid arthritis, chronic obstructive pulmonary disease, cardiovascular diseases, and diabetes (Ruiz *et al*, 2018). It may be noted that the MK2 inhibitor or MK2 knockout elicited a more profound phenotype that could not be fully reversed by PML deficiency, both in terms of necroptosis *in vitro* and SIRS *in vivo* (Figs 5C and D, and 6C, D, F and G). Almost all anti-necroptotic p-RIPK1[S321] was abrogated in MK2-knockout macrophages (Fig 6A and B), as illustrated by the extensive necroptosis induced by zVAD + AT-406 in *Mk2*$^{-/-}$ BMDMs, relative to WT macrophages (Fig EV3D). Therefore, PML is a modifier of MK2 action, but does

not possess the capacity to regulate the on–off switch. Given the potent consequence of MK2 knockout or MK2 inhibition (Figs 5C, D and F, and 6C, D, F and G), the use of a MK2 inhibitor is likely more appropriate for anti-cancer applications than for autoinflammatory diseases. Increasing PML levels should represent a viable approach to treating diseases caused by excessive activation of the p38-MK2 axis (Wolyniec *et al*, 2013). PML levels may be elevated by specific cytokines such as interferons and IL-6 (Chelbi-Alix *et al*, 1995; Lavau *et al*, 1995; Stadler *et al*, 1995; Hubackova *et al*, 2012) or by targeting PML inhibitors (Wolyniec *et al*, 2013). Further studies in this direction may help establish new therapeutic approaches for MK2-mediated inflammatory diseases.

In summary, we have demonstrated that PML inhibits necroptosis and has identified previously unknown functions of PML in terms of its binding to MK2 and inhibition of the p38 MAPK-MK2 signaling axis, as well as its participation in autocrine production of TNF. Suppression of MK2 activation leads to reduced RIPK1[S321] phosphorylation, enhanced necroptosis, and attenuated MK2-mediated carcinogenesis, illustrating an unappreciated mechanism by which PML can suppress tumors. Its antagonism to the MK2 signaling cascade also places PML at a regulatory stage for controlling MK2-initiated inflammatory diseases. In addition, PML is required for autocrine production of TNF triggered by cIAP1/cIAP-2 inhibition, which further enhances necroptosis induction. Together, our results indicate that PML not only can act as a therapeutic target against cancers but also can act as a regulatory module for controlling inflammatory diseases.

Materials and Methods

Reagents and Tools table

Reagent/Resource	Reference or Source	Identifier or Catalog Number	
Experimental Models			
Frozen *Pml*$^{-/-}$ embryos (*M. musculus*)	NCI-Frederick MMHCC Repository, National Cancer Institute (Frederick, MD)	01XF8, 129/Sv-Pml^{tm1Ppp}	
Pml$^{-/-}$ C57BL/6 (*M. musculus*)	Generated from *Pml*$^{-/-}$ embryos by Transgenic Core Facility, Academia Sinica		
Ripk3$^{-/-}$ C57BL/6 (*M. musculus*)	Transgenic Core Facility, Academia Sinica.	Construction described in Methods and Materials	
Mk2$^{-/-}$ C57BL/6 (*M. musculus*)	Transgenic Core Facility, Academia Sinica.	Construction described in Methods and Materials	
Recombinant DNA			
pLentiLox vector (pLL3.7)	Addgene	Cat # 11795	
AIO-GFP vector	Addgene	Cat # 74119	
AIO-mCherry vector	Addgene	Cat # 74120	
pMSCV-GFP vector	Addgene	Cat # 86537	
pcDNA™4 vector	Invitrogen	Cat # V86320	
Antibodies			
Mouse Monoclonal anti-β-actin	Santa Cruz	#sc-69879 RRID: AB_1119529	WB 1:2,000
Mouse Monoclonal anti-β-tubullin (BT7R)	Invitrogen	#MA5-16308 RRID: AB_2537819	WB 1:1,000
Rabbit polyclonal anti-Cleaved Caspase-3 (Asp175)	Cell Signaling	#9661, RRID:AB_2341188	WB 1:1,000
Mouse Monoclonal anti-caspase 8 (1C12)	Cell Signaling	#9746, RRID:AB_2275120	WB 1:500
Rabbit polyclonal anti-caspase 8 Cleaved Caspase-8 (Asp387) (Mouse Specific)	Cell Signaling	#8592, RRID:AB_10891784	WB 1:1,000
Rabbit polyclonal anti-caspase 8 (Mouse Specific)	Cell Signaling	#4927, RRID:AB_2068301	WB 1:1,000
Rabbit polyclonal anti-caspase 8	Abcam	#ab138485, RRID: N/A	IP 1:200
Mouse Monoclonal anti-FADD (1F7)	Merck Millipore	#05-486, RRID:AB_11212178	WB 1:1,000
Goat Polyclonal anti-FADD (M19)	Santa Cruz	#sc-6036, RRID:AB_2100742	WB 1:1,000, IP 1:200

Reagents and Tools table (continued)

Reagent/Resource	Reference or Source	Identifier or Catalog Number	
Rabbit Polyclonal anti-FADD (H181)	Santa Cruz	#sc-5559, RRID:AB_2100622	WB 1:1,000, IP 1:200
Mouse Monoclonal anti-FLAG® M2	Sigma-Aldrich	#F1804, RRID:AB_262044	IP 1:2,000
Mouse Monoclonal anti-FLAG® M2 Peroxidase (HRP)	Sigma-Aldrich	#A8592, RRID:AB_439702	WB 1:10,000
Mouse Monoclonal anti-GAPDH (G-9)	Santa Cruz	#sc-365062 RRID: AB_10847862	WB 1:2,000
Goat Polyclonal anti-Hsp70	Santa cruz	#sc-1060, RRID:AB_631685	WB 1:2,000
Mouse Monoclonal anti-Hsp90	BD Biosciences	#610418, RRID:AB_397798	WB 1:2,000
Rat Monoclonal anti-HA High Affinity	Roche	#11867423001, RRID:AB_390918	IP 1:2,000
Mouse Monoclonal anti-HA—Peroxidase (HRP)	Sigma-Aldrich	#H6533, RRID:AB_439705	WB 1:2,000
Rabbit Monoclonal anti-phospho-IKKα/β (Ser176/180) (16A6)	Cell Signaling	#2697, RRID:AB_2079382	WB 1:1,000, (Blocking buffer: Immobilon® Block - PO)
Rabbit Polyclonal anti-IKKα/β	Santa Cruz	#sc-7607, RRID:AB_675667	WB 1:1,000
Rabbit Monoclonal anti-phospho-IκBα (Ser32) (14D4)	Cell Signaling	#2859, RRID:AB_561111	WB 1:1,000
Rabbit Polyclonal anti-IκBα	Santa Cruz	#sc-371, RRID:AB_2235952	WB 1:4,000
Rabbit Polyclonal anti-Phospho-SAPK/JNK (Thr183/Tyr185)	Cell Signaling	#9251, RRID:AB_331659	WB 1:2,000 (Blocking buffer: Immobilon® Block - PO)
Mouse Monoclonal anti-JNK (D-2)	Santa Cruz	#sc-7345, RRID:AB_675864	WB 1:1,000
Rabbit Polyclonal anti-MAPKAPK2	Invitrogen	#PA5-17729, RRID: AB_10979499	WB 1:2,000 (Blocking buffer: SuperBlock™ T20) IP 1:200 IF 1:200
Rabbit Polyclonal anti-MAPKAPK2	Cell Signaling	#3042, RRID:AB_10694238	WB 1:1,000
Rabbit Monoclonal anti-phospho-MAPKAPK-2 (Thr334) (27B7)	Cell Signaling	#3007, RRID:AB_490936	WB 1:2,000 (Blocking buffer: Immobilon® Block - PO) IF 1:500
Rat Monoclonal anti-MLKL (3H1)	Merck Millipore	#MABC604, RRID: AB_2820284	WB 1:2,000
Rabbit Monoclonal anti-MLKL (EPR17514)	Abcam	#ab184718, RRID: AB_2755030	WB 1:6,000
Rabbit Monoclonal anti-phospho-MLKL (EPR9514)	Abcam	#ab187091, RRID: AB_2619685	WB 1:6,000 (Blocking buffer: SuperBlock™ T20)
Rabbit Monoclonal anti-phospho-MLKL (EPR9515 (2))	Abcam	#ab196436, RRID: AB_2687465	WB 1:6,000 (Blocking buffer: SuperBlock™ T20)
Rabbit Polyclonal anti-MEK3 (I-20)	Santa Cruz	#sc-960, RRID:AB_631928	WB 1:2,000
Rabbit monoclonal anti-MEK3 + MEK6	Abcam	#ab181555, RRID:N/A	WB 1:2,000
Mouse Monoclonal anti-Myc-Tag (9B11) (HRP Conjugate)	Cell Signaling	#2040, RRID:AB_2148465	WB 1:2,000
Mouse Monoclonal anti-Myc-Tag (9B11)	Cell Signaling	#2276, RRID:AB_331783	IP 1:1,000 IF 1:1,000

Reagents and Tools table (continued)

Reagent/Resource	Reference or Source	Identifier or Catalog Number	
Rabbit Monoclonal anti-phospho-NF-κB p65 (Ser536) (93H1)	Cell Signaling	#3033, RRID:AB_331284	WB 1:4,000 (Blocking buffer: Immobilon® Block - PO)
Mouse Monoclonal anti-NF-κB p65 (L8F6)	Cell Signaling	#6956, RRID:AB_10828935	WB 1:2,000
Rabbit Polyclonal NF-κB2 p100/p52 Antibody	Cell Signaling	#4882, RRID:N/A	WB 1:1,000
Rabbit Polyclonal NIK Antibody	Cell Signaling	#4994, RRID:AB_2297422	WB 1:1,000 (Blocking buffer: SuperBlock™ T20)
Rabbit Polyclonal anti-phospho-p38	Cell Signaling	#9211, RRID:AB_331641	WB 1:2,000 (Blocking buffer: Immobilon® Block - PO) IF 1:1,000
Mouse Polyclonal anti-phospho-p38 (28B10)	Cell Signaling	#9216, RRID:AB_331296	WB 1:2,000 IF 1:500
Rabbit Polyclonal anti-p38α (N-20)	Santa Cruz	#sc-728, RRID:AB_632140	WB 1:2,000 IF 1:250
Mouse Polyclonal anti-p38α (F-9)	Santa Cruz	#sc-271120, RRID:AB_10610261	WB 1:2,000 IF 1:250
Rabbit Polyclonal anti-p38α	Cell Signaling	#9218, RRID:AB_10694846	WB 1:2,000 IP 1:400 IF 1:500
Rabbit Polyclonal anti-phospho-p44/42 MAPK (Erk1/2) (Thr202/Tyr204)	Cell Signaling	#9101, RRID:AB_331646	WB 1:6,000
Rabbit Polyclonal anti-p44/42 MAPK (Erk1/2)	Cell Signaling	#9102, RRID:AB_330744	WB 1:6,000
Mouse Monoclonal anti-PML (PML-97)	Sigma-Aldrich	#P6746, RRID:AB_262120	WB 1:1,000
Rabbit Monoclonal anti-PML [EPR16792]	Abcam	#ab179466, RRID:N/A	WB 1:2,000
Mouse Monoclonal anti-PML (36.1-104)	Merck Millipore	#05-718, RRID:AB_309932	WB 1:2,000 IP 1:200
Mouse Monoclonal anti-RIPK1 (38/RIP)	BD Biosciences	#610459, RRID:AB_397832	WB 1:2,000
Rabbit Monoclonal anti-phospho-RIPK1 (Ser166)	Cell Signaling	#65746, RRID:AB_2799693	WB 1:1,000 (Blocking buffer: Immobilon® Block - PO)
Rabbit Polyclonal anti-phospho-RIPK1 (Ser166)	Cell Signaling	#31122, RRID:AB_2799000	WB 1:1,000 (Blocking buffer: Immobilon® Block - PO)
Rabbit Monoclonal anti-phospho-RIPK1 (Ser166) (E7G6O)	Cell Signaling	#53286, RRID:N/A	WB 1:2,000 (Blocking buffer: Immobilon® Block - PO)
Rabbit Polyclonal anti-phospho-RIPK1 (Ser321) (Mouse Specific)	Cell Signaling	#83613, RRID:AB_2800023	WB 1:4,000 (Blocking buffer: Immobilon® Block - PO)
Rabbit Monoclonal anti-RIPK3 (E1Z1D)	Cell Signaling	#13526, RRID:AB_2687467	WB 1:6000
Rabbit Polyclonal anti-RIPK3	ProSci Inc	#2283, RRID:AB_203256	WB 1:6,000
Rabbit Monoclonal anti-phospho-RIPK3 (Ser227) (EPR9627)	Abcam	#ab209384, RRID:AB_2714035	WB 1:4,000 (Blocking buffer: Immobilon® Block - PO)
Rabbit Monoclonal anti-phospho-RIPK3 (Ser232) (EPR9516(N)-25)	Abcam	#ab195117, RRID:AB_2768156	WB 1:3000 (Blocking buffer: Immobilon® Block - PO)
Rabbit Polyclonal anti-TAK1	Santa Cruz	#sc-7162, RRID:AB_2140223	WB 1:2,000
Rabbit Polyclonal anti-phospho-TAK1 (Thr187)	Cell Signaling	#4536, RRID:AB_330493	WB 1:2,000 (Blocking buffer: Immobilon® Block - PO)
Rabbit Polyclonal anti-phospho-TAK1 (Thr184/187)	Cell Signaling	#4531, RRID:AB_390772	WB 1:2,000 (Blocking buffer: Immobilon® Block - PO)

Reagents and Tools table (continued)

Reagent/Resource	Reference or Source	Identifier or Catalog Number	
Peroxidase AffiniPure Goat Anti-Mouse IgG, light chain specific	Jackson ImmunoResearch	115-035-174, RRID: AB_2338512	WB 1:20,000
Peroxidase AffiniPure Goat Anti-Rabbit IgG (H + L)	Jackson ImmunoResearch	111-035-003, RRID: AB_2313567	WB 1:20,000
Peroxidase AffiniPure Goat Anti-Mouse IgG (H + L)	Jackson ImmunoResearch	115-035-003, RRID: AB_10015289	WB 1:20,000
Peroxidase IgG Fraction Monoclonal Mouse Anti-Goat IgG, light chain specific	Jackson ImmunoResearch	205-032-176, RRID: AB_2339056	WB 1:20,000
Peroxidase IgG Fraction Monoclonal Mouse Anti-Rabbit IgG, light chain specific	Jackson ImmunoResearch	211-032-171, RRID: AB_2339149	WB 1:20,000
Goat anti-Rat IgG, Alexa Fluor 647	Invitrogen	A-21247, RRID:AB_141778	IF 1:2,000
Goat anti-Mouse IgG, Alexa Fluor 488	Invitrogen	A-11001, RRID:AB_2534069	IF 1:500
Donkey anti-Rabbit IgG (H + L), Alexa Fluor 555	Invitrogen	A-31572, RRID:AB_162543	IF 1:500
Chemicals, Enzymes and other reagents			
SuperBlock™ T20 (TBS) Blocking Buffer	Thermo Scientific™	Cat # 37536	
Immobilon® Block - PO (Phosphoprotein Blocker)	Millipore	Cat # WBAVDP001	
Lipofectamine 2000 Transfection Reagent	Invitrogen	Cat # 11668-019	
T-Pro Non-liposome Transfection Reagent II	T-Pro Biotechnology	Cat # JT97-N002M	
DharmaFECT 1 Transfection Reagent	Dharmacon	Cat # T-2001	
AT-406	MedKoo Biosciences	Cat # 204460	
BV6	Adooq bioscience	Cat # A14231	
Z-VAD-FMK	Adooq bioscience	Cat # A12373	
Cycloheximide	Sigma-Aldrich	Cat # C4859	
7-Cl-O-Nec1 (Nec-1s)	Abcam	Cat # ab221984	
Necrostatin-1	Sigma-Aldrich	Cat # N9037	
PF-3644022 hydrate	Sigma-Aldrich	Cat # PZ0188	
WesternBright ECL HRP substrate	Advansta	Cat # K-12045-D50	
WesternBright Sirius HRP substrate	Advansta	Cat # K-12043-D20	
Mix-n-Stain™ Enzyme Antibody Labeling Kits	Biotium	Cat # 92300	
EverBrite™ Hardset Mounting Medium with DAPI	Biotium	Cat # 23004	
Protein A/G PLUS-Agarose	Santa cruz	Cat # sc-2003	
Recombinant Human TNF-α	PeproTech	Cat # 300-01A	
Recombinant Murine TNF-α	PeproTech	Cat # 315-01A	
Recombinant human p38 protein	Abcam	Cat # ab82188	
Recombinant human MK2 protein	Abcam	Cat # ab60307	
Software			
GraphPad Prism 6	https://www.graphpad.com/		
Other			
CellTiter-Glo® Luminescent Cell Viability Assay kit	Promega	Cat # G7570	
LDH Cytotoxicity Detection Kit	Clontech	Cat # MK401	
FUJI DRI-CHEM SLIDE GPT/ALT-P III	FUJI	Cat # 15809554	
Thiazolyl Blue Tetrazolium Bromide (MTT)	Sigma-Aldrich	Cat # M2128	
Propidium iodide	Sigma-Aldrich	Cat #P4170	

Methods and Protocols

PML-knockout and MK2-knockout mice

PML-knockout mice were generated previously (Wang *et al*, 1998). Frozen *Pml*$^{-/-}$ embryos (01XF8, 129/Sv-Pml^{tm1Ppp}) were obtained from the NCI-Frederick MMHCC Repository, National Cancer Institute (Frederick, MD). Generation of *Pml*$^{-/-}$ mice from *Pml*$^{-/-}$ frozen embryos was conducted as described previously (Lo *et al*, 2013). Mice used in this study were back-crossed with C57BL/6 mice for 12 generations or more. *Pml*$^{-/-}$ mice were maintained by breeding *Pml*$^{+/-}$ mice to generate *Pml*$^{+/+}$ and *Pml*$^{-/-}$ mice. *Ripk3*$^{-/-}$ mice were generated using a CRISPR-Cas9 approach by the Transgenic Core Facility, Academia Sinica. The following sequences were used: sgRNA target 1, 5'-GTCTGTGCACACATAACTCCAGG-3'; sgRNA target 2, 5'-ACAGGCCTAATGCACCCTCACGG-3'. RIPK3 genomic DNA typing was performed by polymerase chain reaction (PCR) using the following primers: RIPK3-fwd, 5'-GGAGCCTCTTATTT GAAAGG-3' and RIPK3-rev, 5'-GACAGGCCAAAATCTGCTAG-3', generating PCR products of 410 base pairs (bps) for the knockout allele or 1,400 bps for the WT allele. *Mk2*-knockout mice in C57BL/6J background were generated using a CRISPR-Cas9 approach by the Transgenic Core Facility, Academia Sinica. The sgRNA were designed to target to *Mk2* intron 2 (target sequence: GAAAACATTTG-TAGTGTTGG) and intron 3 (target sequence: CCAAGCTTCAAGATC-CATAG). Knockout mice in which exon 3 of *Mk2* was deleted were confirmed by genomic sequencing. PCR using primer sequences (forward-5' TCCTTTTGTTCTGACTCCGTGG; reverse-5' GAGGCC-CATGGCCAGCAGT) for mice genotyping generated PCR products of 634 bps for the knockout allele and 910 bps for the WT allele. Mice were maintained in the SPF mouse facility of the Institute of Molecular Biology, Academia Sinica, with ambient temperature at 21°C, humidity of 55%, dark/light cycle of 10 h/14 h, and air exchange rate of 12-15 times per hour. All mouse experiments were conducted with approval from the Institutional Animal Care & Utilization Committee, Academia Sinica.

Cell culture

Murine bone marrow cells were flushed out from tibias and femurs by cold RPMI medium, and the red blood cells were lysed and then cultured in DMEM with 10% FBS (Invitrogen/Life Technologies), 10 mM glutamine, 100 U/ml penicillin, 100 μg/ml streptomycin, and 50 μM 2-ME (complete DMEM), with an additional 20% L929 cell-conditioned medium to generate bone marrow-derived macrophages (BMDMs). For cell surface marker expression, BMDMs were detached from dishes using a cell lifter, and stained with anti-CD11b-PE-Cy7, anti-F4/80-eFluor 450, anti-CD80-APC, and anti-CD206-FITC, and then analyzed on an aBD™ LSR II flow cytometer. Live cells were gated from SSC/FSC, and macrophages were then gated by CD11b^{+}F4/80^{+}, with CD80^{+} designated as M1 macrophages and CD206^{+} designated as M2 macrophages. BMDMs used in this study were confirmed to be M1 macrophages. The human colon adenocarcinoma cell line HT-29 was cultured in complete RPMI-1640 medium with the same supplements as for complete DMEM. *Pml*$^{+/+}$ and *Pml*$^{-/-}$ mouse embryonic fibroblasts were gifts of Dr. Gerd G. Maul (Wistar Institute, Philadelphia) and were cultured in complete DMEM (Ishov *et al*, 2004). Murine peritoneal macrophages were isolated from thioglycollate-elicited mice and were cultured in complete DMEM.

PML-knockdown HT-29 cells

The PML-knockdown lentiviral construct was generated by subcloning a PML-specific shRNA sequence into pLentiLox vector (pLL3.7). The target sequence was 5'-GAGTCGGCCGACTTCTGGT-3'. Lentiviruses were harvested from culture supernatant of HEK293T cells transfected with 20 μg pLL3.7 or pLL3.7-PMLsiRNA, 15 μg psPAX2, and 6 μg pMD2.G. HT-29 cells were infected with recombinant lentivirus, and GFP-expressing cells were then isolated by fluorescence sorting 48 h later. Levels of PML were confirmed by immunoblotting.

PML- and MK2-knockout U937 and HT-29 cells

Human *PML* or human *MK2* gRNA sequences were cloned into AIO-GFP or AIO-mCherry vector. The *PML* exon 1 target sequences were sense 5'-CTGCACCCGCCCGATCTCCG and antisense 5'-CCCAGCT TAGTTTCGATTCT. The *PML* exon 2 target sequences were sense 5'-GTCGGTGTACCGGCAGATTG and antisense 5'-TCTCGAAAAA GACGTTATCC. The *MK2* #1 target sequences were sense 5'-CCGC AGTTCCACGTCAAGTC and antisense 5'-TTTGAGGGCGAATTTC TCCT, and for *MK2* #2, they were sense 5'-CCCTGCCCTGCCGCA CCCCC and antisense 5'-GGGACGCCGGGGCACAGGCG. U937 and HT-29 cells were transfected with gRNA-containing AIO-GFP or AIO-mCherry plasmids, and GFP- or mCherry-expressing cells were isolated by fluorescence sorting. The monoclonal cell line was cultured, and protein expression was verified by Western blotting.

Primary MEFs

Pml$^{+/-}$*Mk2*$^{+/-}$ male and female mice were crossed, and the individual embryos were collected and genotyped at pregnancy day 13.5. WT, *Pml*$^{-/-}$, *Mk2*$^{-/-}$, and *Pml*$^{-/-}$*Mk2*$^{-/-}$ embryo were trypsinized and filtered, and then, mouse embryonic fibroblasts were used for further studies.

Ripk1-knockout MEFs

Mouse *Ripk1* gRNA sequences were cloned into AIO-GFP or AIO-mCherry vector. The *Ripk1* #1 target sequences were sense 5'-AAGTCGGACGTGTACAGCTT and antisense 5'-TGTGAAAGTCAC GATCAACG, and for *Ripk1* #2, they were sense 5'-AGAATATGT AGAAGAGGATG and antisense 5'-TCTCCCTTGGACAGTACTCA. Immortalized mouse WT MEFs or *Pml*-knockout MEFs were transfected with *Ripk1* gRNA-containing AIO-GFP or AIO-mCherry plasmids. The monoclonal cell line was cultured, and protein expression was verified by Western blotting.

RIPK1 reconstitution

WT *Ripk1* and *Ripk1* [S336A] were subcloned into pMSCV vector and transfected into HEK293T cells. The *Ripk1*-containing viruses were collected 48 h after transfection, and virus supernatant was used to transduce *Ripk1*-knockout MEFs. Protein expression was verified by Western blotting.

Knockdown of p38 MAPK

p38 MAPK was knocked down in MEF cells using siGenome mouse MAPK14-SMARTpool (Dharmacon) with four target sequences: #1 GGAAGAGCCUGACCUAUGA, #2 GCAAGAAACUA CAUUCAGU, #3 GUACAGACCAUAUUGAUCA, and #4 GGGCUG AAGUAUAUACAUU.

Immunofluorescence

For immunofluorescence staining, cells were seeded on coverslips in 24 wells. BMDM cells were treated as indicated, washed with warm PBS, and fixed by 4% paraformaldehyde at 37°C. For MK2-, PML-, and p38 MAPK-overexpressing HEK293T cells, the cells were seeded 24 h after transfection onto coverslips overnight before fixation. Fixed cells were permeabilized and stained with primary antibodies at 4°C overnight, followed by labeled secondary antibodies for 1 h at room temperature. EverBrite™ Hardset Mounting Medium with DAPI (Biotium, 23004) was used for cell nucleus staining. Fluorescence images were obtained with a Zeiss LSM780 confocal microscope (Carl Zeiss, Jena, Germany), and fluorescence intensities were quantified by Zeiss Zen microscope software. The pinhole setup of the LSM780 confocal microscope was 1.92 airy units (2.6 μm) per section under a 40×/1.4 oil DIC M27 objective and 0.88 airy units (2.0 μm) per section under a 63×/1.4 oil DIC M27 objective. The excitation wavelength was 405 nm for DAPI, 488 nm for Alexa Fluor 488, and 561 nm for Alexa Fluor 555.

Cell viability assay

BMDMs from wild-type or *Pml*-knockout mice were seeded into 96-well plates for 2 h and treated with zVAD (20 μM) or AT-406 (0.5 μM), with or without Nec-1 (40 μM), for 18 h in our ATP cell viability assay and for 16 h in our MTT cell viability assay. ATP cell viability assays were conducted using a CellTiter-Glo® Luminescent Cell Viability Assay kit (Promega, G7570). For our MTT assays, the MTT reagent was added and incubated for 4 h at 37°C. The intensity of purple formazan formed was measured by absorbance at 490 nm on an Emax microtiter plate reader (Molecular Device, Sunnyvale, CA). HT-29 cells were seeded into a 12-well plate overnight and treated with human TNF (5 ng/ml), zVAD (20 μM), and BV6 (0.5 μM), with or without Nec-1 (40 μM), for 16 h. Cells were trypsinized and cell death was determined by propidium iodide staining, with quantitation performed using a flow cytometer.

Immunoblotting

For immunoblotting, cells were washed by PBS and lysed in 0.1% Triton X-100 lysis buffer (0.1% Triton X-100, 25 mM HEPES, 300 mM NaCl, 1.5 mM $MgCl_2$, 0.2 mM EDTA, 0.5 mM DTT, 0.1 mM Na_3VO_4, and 50 mM NaF) or 0.2% NP-40 buffer (0.2% NP-40, 10 mM Tris–HCl, 120 mM NaCl). Cell lysates were centrifuged at 12,000 × *g* for 15 min, and supernatants were mixed with 2- or 5-fold sample buffer at 95°C for 5 min. The proteins were resolved by SDS–PAGE and transferred to PVDF membranes. For specific protein staining, membranes were blocked by 5% low-fat milk (in TBST containing 10 mM Tris–HCl pH 8.0, 150 mM NaCl, 0.05% Tween 20) at room temperature for 1 h and stained with primary antibodies overnight at 4°C or 4 h at room temperature. Membranes were washed three times with TBST and incubated with horseradish peroxidase (HRP)-conjugated secondary antibodies for 1 h at room temperature. The membrane was developed with WesternBright ECL HRP substrate (Advansta), and chemiluminescence was detected by X-ray film (FUJIFILM).

Immunoprecipitation

For FADD complex pull-down, cells were washed and lysed in 0.1% Triton X-100 lysis buffer (0.1% Triton X-100, 25 mM HEPES, 300 mM NaCl, 1.5 mM $MgCl_2$, 0.2 mM EDTA, 0.5 mM DTT, 0.1 mM Na_3VO_4, and 50 mM NaF) with protease inhibitor cocktail (Thermo, #78430) for 30 min on ice. Cell lysates were centrifuged at 12,000 *g* for 15 min, and supernatants were incubated with FADD antibody overnight at 4°C, followed by Protein G Sepharose for 1 h. Beads were washed with lysis buffer, and the associated proteins were detected by Western blotting. For MK2, p38, MKK3, and PML complex pull-down from total cell lysates, cells were lysed in 0.2% NP-40 buffer (0.2% NP-40, 10 mM Tris–HCl, 120 mM NaCl) with protease inhibitor cocktail.

TNF-induced septic shock

Wild-type or *Pml*-knockout C57BL/6 mice aged 6–8 weeks and of the same sex were used for TNF-induced septic shock. Mice were anesthetized using Avertin, and mouse TNF (1.5 μg/g) in a total volume of 200 μl endotoxin-free PBS was injected intravenously (i.v.). Body temperatures were monitored rectally every 1–3 h for 30 h using an industrial electronic thermometer (Kane-May), and mouse mortality was recorded at the same time. Mice were sacrificed when their body temperature fell below 22°C. Serum was collected by cardiac puncture 15 min within mice dying. For live mice, serum was collected 30 h after TNF injection. Serum LDH was measured using an LDH Cytotoxicity Detection Kit (Clontech, #MK401) following the user manual. Serum GPT/ALT levels were determined using FUJI DRI-CHEM SLIDE GPT/ALT-P III (FUJIFILM, Tokyo, Japan). Mouse serum TNF, IL-6, and IL-1α levels were detected using a TNF alpha Mouse Uncoated ELISA Kit (Invitrogen, #88-7324-88), IL-6 Mouse Uncoated ELISA Kit (Invitrogen, #88-7064-88), or ELISA MAX™ Deluxe Set Mouse IL-1α (BioLegend, #433404), respectively. For MK2 and RIPK1 inhibitor treatment, mice were pre-treated with 75 μg PF-3644022 (Sigma-Aldrich, # PZ0188) per mouse or Nec-1s (6 μg/g) 15 min before TNF injection by intraperitoneal injection, and then subjected to inhibitor treatment again 60 min after TNF injection.

Statistics

GraphPad Prism 6 and Microsoft Office Excel were used for data analyses. Unpaired two-tailed Student's *t*-tests were used to compare results between two groups. Data are presented as mean with standard deviation (SD) or standard error of the mean (SEM). Body temperature decline was analyzed by two-way ANOVA for multiple comparisons. A log-rank (Mantel–Cox) test was used to statistically compare survival curves. Confocal images were quantitated using Zeiss Zen or ImageJ. Phosphoprotein was quantitated using ImageJ. P-values < 0.05 were considered significant.

Data availability

This study includes no data deposited in external repositories.

Expanded View for this article is available online.

Acknowledgements

We thank Dr. Ching-Yen Tsai and staff of the Transgenic Core Facility of Academia Sinica for generating the RIPK3-knockout and MK2-knockout mouse lines, Yamin Lin and staff of the FACS Core of the Institute of Molecular Biology Academia Sinica (IMB) for cell sorting, Sue-Ping Lee and staff of the Confocal Core of IMB for confocal microscopy, and Dr. John O'Brien for editing the

manuscript. This work was supported by Academia Sinica and grant MOST 109-2326-B-001-008 from the Ministry of Science and Technology, Taiwan, R.O.C.

Author contributions

ITC and HCC contributed to data acquisition, analyzed and interpreted the data, and statistically analyzed the data; YHL, PYL, FYH, and YHW contributed to data acquisition and analyzed the data; HMS and MZL drafted the manuscript; MZL involved in study concept and design, and supervised the study.

Conflict of interest

The authors declare that they have no conflict of interest.

References

Ahmed A, Wan X, Mitxitorena I, Lindsay AJ, Paolo Pandolfi P, McCaffrey MW, Keeshan K, Chen YH, Carmody RJ (2017) Regulation of NF-kappaB by PML and PML-RARalpha. *Sci Rep* 7: 44539

Annibaldi A, Meier P (2018) Checkpoints in TNF-induced cell death: implications in inflammation and cancer. *Trends Mol Med* 24: 49 – 65

Banani SF, Rice AM, Peeples WB, Lin Y, Jain S, Parker R, Rosen MK (2016) Compositional control of phase-separated cellular bodies. *Cell* 166: 651 – 663

Bellodi C, Kindle K, Bernassola F, Cossarizza A, Dinsdale D, Melino G, Heery D, Salomoni P (2006) A cytoplasmic PML mutant inhibits p53 function. *Cell Cycle* 5: 2688 – 2692

Ben-Levy R, Hooper S, Wilson R, Paterson HF, Marshall CJ (1998) Nuclear export of the stress-activated protein kinase p38 mediated by its substrate MAPKAP kinase-2. *Curr Biol* 8: 1049 – 1057

Bernardi R, Pandolfi PP (2007) Structure, dynamics and functions of promyelocytic leukaemia nuclear bodies. *Nat Rev Mol Cell Biol* 8: 1006 – 1016

Bernardi R, Papa A, Pandolfi PP (2008) Regulation of apoptosis by PML and the PML-NBs. *Oncogene* 27: 6299 – 6312

Bernardi R, Scaglioni PP, Bergmann S, Horn HF, Vousden KH, Pandolfi PP (2004) PML regulates p53 stability by sequestering Mdm2 to the nucleolus. *Nat Cell Biol* 6: 665 – 672

Bertrand MJ, Milutinovic S, Dickson KM, Ho WC, Boudreault A, Durkin J, Gillard JW, Jaquith JB, Morris SJ, Barker PA (2008) cIAP1 and cIAP2 facilitate cancer cell survival by functioning as E3 ligases that promote RIP1 ubiquitination. *Mol Cell* 30: 689 – 700

Cai Q, Sun H, Peng Y, Lu J, Nikolovska-Coleska Z, McEachern D, Liu L, Qiu SU, Yang C-Y, Miller R *et al* (2011) A potent and orally active antagonist (SM-406/AT-406) of multiple inhibitor of apoptosis proteins (IAPs) in clinical development for cancer treatment. *J Med Chem* 54: 2714 – 2726

Cai Z, Jitkaew S, Zhao J, Chiang HC, Choksi S, Liu J, Ward Y, Wu LG, Liu ZG (2014) Plasma membrane translocation of trimerized MLKL protein is required for TNF-induced necroptosis. *Nat Cell Biol* 16: 55 – 65

Chan FK, Luz NF, Moriwaki K (2015) Programmed necrosis in the cross talk of cell death and inflammation. *Annu Rev Immunol* 33: 79 – 106

Chelbi-Alix MK, Pelicano L, Quignon F, Koken MH, Venturini L, Stadler M, Pavlovic J, Degos L, de The H (1995) Induction of the PML protein by interferons in normal and APL cells. *Leukemia* 9: 2027 – 2033

Chen X, Li W, Ren J, Huang D, He W-T, Song Y, Yang C, Li W, Zheng X, Chen P *et al* (2014) Translocation of mixed lineage kinase domain-like protein to plasma membrane leads to necrotic cell death. *Cell Res* 24: 105 – 121

Cho YS, Challa S, Moquin D, Genga R, Ray TD, Guildford M, Chan FK (2009) Phosphorylation-driven assembly of the RIP1-RIP3 complex regulates programmed necrosis and virus-induced inflammation. *Cell* 137: 1112 – 1123

Condemine W, Takahashi Y, Zhu J, Puvion-Dutilleul F, Guegan S, Janin A, de The H (2006) Characterization of endogenous human promyelocytic leukemia isoforms. *Cancer Res* 66: 6192 – 6198

Degterev A, Hitomi J, Germscheid M, Ch'en IL, Korkina O, Teng X, Abbott D, Cuny GD, Yuan C, Wagner G *et al* (2008) Identification of RIP1 kinase as a specific cellular target of necrostatins. *Nat Chem Biol* 4: 313 – 321

Dillon C, Weinlich R, Rodriguez D, Cripps J, Quarato G, Gurung P, Verbist K, Brewer T, Llambi F, Gong Y-N *et al* (2014) RIPK1 blocks early postnatal lethality mediated by caspase-8 and RIPK3. *Cell* 157: 1189 – 1202

Dondelinger Y, Aguileta MA, Goossens V, Dubuisson C, Grootjans S, Dejardin E, Vandenabeele P, Bertrand MJ (2013) RIPK3 contributes to TNFR1-mediated RIPK1 kinase-dependent apoptosis in conditions of cIAP1/2 depletion or TAK1 kinase inhibition. *Cell Death Differ* 20: 1381 – 1392

Dondelinger Y, Delanghe T, Rojas-Rivera D, Priem D, Delvaeye T, Bruggeman I, Van Herreweghe F, Vandenabeele P, Bertrand MJM (2017) MK2 phosphorylation of RIPK1 regulates TNF-mediated cell death. *Nat Cell Biol* 19: 1237 – 1247

Dondelinger Y, Jouan-Lanhouet S, Divert T, Theatre E, Bertin J, Gough PJ, Giansanti P, Heck AJ, Dejardin E, Vandenabeele P *et al* (2015) NF-kappaB-independent role of IKKalpha/IKKbeta in preventing RIPK1 kinase-dependent apoptotic and necroptotic cell death during TNF signaling. *Mol Cell* 60: 63 – 76

Doucas V, Tini M, Egan DA, Evans RM (1999) Modulation of CREB binding protein function by the promyelocytic (PML) oncoprotein suggests a role for nuclear bodies in hormone signaling. *Proc Natl Acad Sci USA* 96: 2627 – 2632

Duprez L, Takahashi N, Van Hauwermeiren F, Vandendriessche B, Goossens V, Vanden Berghe T, Declercq W, Libert C, Cauwels A, Vandenabeele P (2011) RIP Kinase-dependent necrosis drives lethal systemic inflammatory response syndrome. *Immunity* 35: 908 – 918

Engel K, Kotlyarov A, Gaestel M (1998) Leptomycin B-sensitive nuclear export of MAPKAP kinase 2 is regulated by phosphorylation. *Embo J* 17: 3363 – 3371

Feng X, Song Q, Yu A, Tang H, Peng Z, Wang X (2015) Receptor-interacting protein kinase 3 is a predictor of survival and plays a tumor suppressive role in colorectal cancer. *Neoplasma* 62: 592 – 601

Galluzzi L, Kepp O, Chan FK, Kroemer G (2017) Necroptosis: mechanisms and relevance to disease. *Annu Rev Pathol* 12: 103 – 130

Galluzzi L, Vitale I, Aaronson SA, Abrams JM, Adam D, Agostinis P, Alnemri ES, Altucci L, Amelio I, Andrews DW *et al* (2018) Molecular mechanisms of cell death: recommendations of the Nomenclature Committee on Cell Death 2018. *Cell Death Differ* 25: 486 – 541

Gentric G, Kieffer Y, Mieulet V, Goundiam O, Bonneau C, Nemati F, Hurbain I, Raposo G, Popova T, Stern M-H *et al* (2019) PML-regulated mitochondrial metabolism enhances chemosensitivity in human ovarian cancers. *Cell Metab* 29: 156 – 173.e10

Gerlach B, Cordier SM, Schmukle AC, Emmerich CH, Rieser E, Haas TL, Webb AI, Rickard JA, Anderton H, Wong W-L *et al* (2011) Linear ubiquitination prevents inflammation and regulates immune signalling. *Nature* 471: 591 – 596

Giorgi C, Ito K, Lin H-K, Santangelo C, Wieckowski MR, Lebiedzinska M, Bononi A, Bonora M, Duszynski J, Bernardi R *et al* (2010) PML regulates apoptosis at endoplasmic reticulum by modulating calcium release. *Science* 330: 1247 – 1251

Gurrieri C, Capodieci P, Bernardi R, Scaglioni PP, Nafa K, Rush LJ, Verbel DA, Cordon-Cardo C, Pandolfi PP (2004) Loss of the tumor suppressor PML in human cancers of multiple histologic origins. *J Natl Cancer Inst* 96: 269 – 279

Han J, Wu J, Silke J (2020) An overview of mammalian p38 mitogen-activated protein kinases, central regulators of cell stress and receptor signaling. *F1000Res* 9: 653

He S, Wang L, Miao L, Wang T, Du F, Zhao L, Wang X (2009) Receptor interacting protein kinase-3 determines cellular necrotic response to TNF-alpha. *Cell* 137: 1100 – 1111

Henriques A, Koliaraki V, Kollias G (2018) Mesenchymal MAPKAPK2/HSP27 drives intestinal carcinogenesis. *Proc Natl Acad Sci USA* 115: E5546 – E5555

Hildebrand JM, Tanzer MC, Lucet IS, Young SN, Spall SK, Sharma P, Pierotti C, Garnier J-M, Dobson RCJ, Webb AI *et al* (2014) Activation of the pseudokinase MLKL unleashes the four-helix bundle domain to induce membrane localization and necroptotic cell death. *Proc Natl Acad Sci USA* 111: 15072 – 15077

Hitti E, Iakovleva T, Brook M, Deppenmeier S, Gruber AD, Radzioch D, Clark AR, Blackshear PJ, Kotlyarov A, Gaestel M (2006) Mitogen-activated protein kinase-activated protein kinase 2 regulates tumor necrosis factor mRNA stability and translation mainly by altering tristetraprolin expression, stability, and binding to adenine/uridine-rich element. *Mol Cell Biol* 26: 2399 – 2407

Hsu KS, Guan BJ, Cheng X, Guan D, Lam M, Hatzoglou M, Kao HY (2016) Translational control of PML contributes to TNFalpha-induced apoptosis of MCF7 breast cancer cells and decreased angiogenesis in HUVECs. *Cell Death Differ* 23: 469 – 483

Hubackova S, Krejcikova K, Bartek J, Hodny Z (2012) Interleukin 6 signaling regulates promyelocytic leukemia protein gene expression in human normal and cancer cells. *J Biol Chem* 287: 26702 – 26714

Ikeda F, Deribe YL, Skanland SS, Stieglitz B, Grabbe C, Franz-Wachtel M, van Wijk SJ, Goswami P, Nagy V, Terzic J *et al* (2011) SHARPIN forms a linear ubiquitin ligase complex regulating NF-kappaB activity and apoptosis. *Nature* 471: 637 – 641

Ishov AM, Vladimirova OV, Maul GG (2004) Heterochromatin and ND10 are cell-cycle regulated and phosphorylation-dependent alternate nuclear sites of the transcription repressor Daxx and SWI/SNF protein ATRX. *J Cell Sci* 117: 3807 – 3820

Jaco I, Annibaldi A, Lalaoui N, Wilson R, Tenev T, Laurien L, Kim C, Jamal K, Wicky John S, Liccardi G *et al* (2017) MK2 phosphorylates RIPK1 to prevent TNF-induced cell death. *Mol Cell* 66: 698 – 710.e5

Kaiser WJ, Daley-Bauer LP, Thapa RJ, Mandal P, Berger SB, Huang C, Sundararajan A, Guo H, Roback L, Speck SH *et al* (2014) RIP1 suppresses innate immune necrotic as well as apoptotic cell death during mammalian parturition. *Proc Natl Acad Sci USA* 111: 7753 – 7758

Kaiser WJ, Upton JW, Long AB, Livingston-Rosanoff D, Daley-Bauer LP, Hakem R, Caspary T, Mocarski ES (2011) RIP3 mediates the embryonic lethality of caspase-8-deficient mice. *Nature* 471: 368 – 372

Kearney CJ, Martin SJ (2017) An inflammatory perspective on necroptosis. *Mol Cell* 65: 965 – 973

Koo G-B, Morgan MJ, Lee D-G, Kim W-J, Yoon J-H, Koo JS, Kim SI, Kim SJ, Son MK, Hong SS *et al* (2015) Methylation-dependent loss of RIP3 expression in cancer represses programmed necrosis in response to chemotherapeutics. *Cell Res* 25: 707 – 725

Krysko O, Aaes TL, Kagan VE, D'Herde K, Bachert C, Leybaert L, Vandenabeele P, Krysko DV (2017) Necroptotic cell death in anti-cancer therapy. *Immunol Rev* 280: 207 – 219

Lalaoui N, Brumatti G (2017) Relevance of necroptosis in cancer. *Immunol Cell Biol* 95: 137 – 145

Lalaoui N, Hänggi K, Brumatti G, Chau D, Nguyen N-YN, Vasilikos L, Spilgies L, Heckmann D, Ma C, Ghisi M *et al* (2016) Targeting p38 or MK2 enhances the anti-leukemic activity of Smac-mimetics. *Cancer Cell* 29: 145 – 158

Lallemand-Breitenbach V, de The H (2018) PML nuclear bodies: from architecture to function. *Curr Opin Cell Biol* 52: 154 – 161

Lavau C, Marchio A, Fagioli M, Jansen J, Falini B, Lebon P, Grosveld F, Pandolfi PP, Pelicci PG, Dejean A (1995) The acute promyelocytic leukaemia-associated PML gene is induced by interferon. *Oncogene* 11: 871 – 876

Li H, Leo C, Zhu J, Wu X, O'Neil J, Park EJ, Chen JD (2000) Sequestration and inhibition of Daxx-mediated transcriptional repression by PML. *Mol Cell Biol* 20: 1784 – 1796

Lin DY, Lai MZ, Ann DK, Shih HM (2003) Promyelocytic leukemia protein (PML) functions as a glucocorticoid receptor co-activator by sequestering Daxx to the PML oncogenic domains (PODs) to enhance its transactivation potential. *J Biol Chem* 278: 15958 – 15965

Lin HK, Bergmann S, Pandolfi PP (2004) Cytoplasmic PML function in TGF-beta signalling. *Nature* 431: 205 – 211

Lo Y-H, Huang Y-W, Wu Y-H, Tsai C-S, Lin Y-C, Mo S-T, Kuo W-C, Chuang Y-T, Jiang S-T, Shih H-M *et al* (2013) Selective inhibition of the NLRP3 inflammasome by targeting to promyelocytic leukemia protein in mouse and human. *Blood* 121: 3185 – 3194

Maarifi G, Chelbi-Alix MK, Nisole S (2014) PML control of cytokine signaling. *Cytokine Growth Factor Rev* 25: 551 – 561

Mahoney DJ, Cheung HH, Mrad RL, Plenchette S, Simard C, Enwere E, Arora V, Mak TW, Lacasse EC, Waring J *et al* (2008) Both cIAP1 and cIAP2 regulate TNFalpha-mediated NF-kappaB activation. *Proc Natl Acad Sci USA* 105: 11778 – 11783

Menon MB, Gaestel M (2018) MK2-TNF-signaling comes full circle. *Trends Biochem Sci* 43: 170 – 179

Menon MB, Gropengiesser J, Fischer J, Novikova L, Deuretzbacher A, Lafera J, Schimmeck H, Czymmeck N, Ronkina N, Kotlyarov A *et al* (2017) p38 (MAPK)/MK2-dependent phosphorylation controls cytotoxic RIPK1 signalling in inflammation and infection. *Nat Cell Biol* 19: 1248 – 1259

Mohamad N, Boden M (2010) The proteins of intra-nuclear bodies: a data-driven analysis of sequence, interaction and expression. *BMC Syst Biol* 4: 44

Murphy J, Czabotar P, Hildebrand J, Lucet I, Zhang J-G, Alvarez-Diaz S, Lewis R, Lalaoui N, Metcalf D, Webb A *et al* (2013) The pseudokinase MLKL mediates necroptosis via a molecular switch mechanism. *Immunity* 39: 443 – 453

Najafov A, Chen H, Yuan J (2017) Necroptosis and cancer. *Trends Cancer* 3: 294 – 301

Newton K, Dugger DL, Maltzman A, Greve JM, Hedehus M, Martin-McNulty B, Carano RAD, Cao TC, van Bruggen N, Bernstein L *et al* (2016) RIPK3 deficiency or catalytically inactive RIPK1 provides greater benefit than MLKL deficiency in mouse models of inflammation and tissue injury. *Cell Death Differ* 23: 1565 – 1576

Niwa-Kawakita M, Ferhi O, Soilihi H, Le Bras M, Lallemand-Breitenbach V, de The H (2017) PML is a ROS sensor activating p53 upon oxidative stress. *J Exp Med* 214: 3197 – 3206

Nugues AL, El Bouazzati H, Hetuin D, Berthon C, Loyens A, Bertrand E, Jouy N, Idziorek T, Quesnel B (2014) RIP3 is downregulated in human myeloid leukemia cells and modulates apoptosis and caspase-mediated p65/RelA cleavage. *Cell Death Dis* 5: e1384

Oberst A, Dillon CP, Weinlich R, McCormick LL, Fitzgerald P, Pop C, Hakem R, Salvesen GS, Green DR (2011) Catalytic activity of the caspase-8-FLIP(L) complex inhibits RIPK3-dependent necrosis. *Nature* 471: 363 – 367

Pasparakis M, Vandenabeele P (2015) Necroptosis and its role in inflammation. *Nature* 517: 311 – 320

Polykratis A, Hermance N, Zelic M, Roderick J, Kim C, Van TM, Lee TH, Chan FKM, Pasparakis M, Kelliher MA (2014) Cutting edge: RIPK1 Kinase inactive mice are viable and protected from TNF-induced necroptosis in vivo. *J Immunol* 193: 1539 – 1543

Renner F, Moreno R, Schmitz ML (2010) SUMOylation-dependent localization of IKKepsilon in PML nuclear bodies is essential for protection against DNA-damage-triggered cell death. *Mol Cell* 37: 503 – 515

Rickard J, O'Donnell J, Evans J, Lalaoui N, Poh A, Rogers TeWhiti, Vince J, Lawlor K, Ninnis R, Anderton H *et al* (2014) RIPK1 regulates RIPK3-MLKL-driven systemic inflammation and emergency hematopoiesis. *Cell* 157: 1175 – 1188

Robinson N, McComb S, Mulligan R, Dudani R, Krishnan L, Sad S (2012) Type I interferon induces necroptosis in macrophages during infection with *Salmonella enterica serovar* Typhimurium. *Nat Immunol* 13: 954 – 962

Ruiz M, Coderre L, Allen BG, Desrosiers C (2018) Protecting the heart through MK2 modulation, toward a role in diabetic cardiomyopathy and lipid metabolism. *Biochim Biophys Acta Mol Basis Dis* 1864: 1914 – 1922

Sahin U, Ferhi O, Jeanne M, Benhenda S, Berthier C, Jollivet F, Niwa-Kawakita M, Faklaris O, Setterblad N, de Thé H *et al* (2014) Oxidative stress-induced assembly of PML nuclear bodies controls sumoylation of partner proteins. *J Cell Biol* 204: 931 – 945

Salomoni P, Pandolfi PP (2002) The role of PML in tumor suppression. *Cell* 108: 165 – 170

Sato S, Sanjo H, Takeda K, Ninomiya-Tsuji J, Yamamoto M, Kawai T, Matsumoto K, Takeuchi O, Akira S (2005) Essential function for the kinase TAK1 in innate and adaptive immune responses. *Nat Immunol* 6: 1087 – 1095

Shim JH, Xiao C, Paschal AE, Bailey ST, Rao P, Hayden MS, Lee KY, Bussey C, Steckel M, Tanaka N *et al* (2005) TAK1, but not TAB1 or TAB2, plays an essential role in multiple signaling pathways in vivo. *Genes Dev* 19: 2668 – 2681

Shin J, Park B, Cho S, Lee S, Kim Y, Lee S-O, Cho K, Lee S, Jin B-S, Ahn J-H *et al* (2004) Promyelocytic leukemia is a direct inhibitor of SAPK2/p38 mitogen-activated protein kinase. *J Biol Chem* 279: 40994 – 41003

Stadler M, Chelbi-Alix MK, Koken MH, Venturini L, Lee C, Saib A, Quignon F, Pelicano L, Guillemin MC, Schindler C *et al* (1995) Transcriptional induction of the PML growth suppressor gene by interferons is mediated through an ISRE and a GAS element. *Oncogene* 11: 2565 – 2573

Su Z, Yang Z, Xie L, DeWitt JP, Chen Y (2016) Cancer therapy in the necroptosis era. *Cell Death Differ* 23: 748 – 756

Suarez-Lopez L, Sriram G, Kong YW, Morandell S, Merrick KA, Hernandez Y, Haigis KM, Yaffe MB (2018) MK2 contributes to tumor progression by promoting M2 macrophage polarization and tumor angiogenesis. *Proc Natl Acad Sci USA* 115: E4236 – E4244

Sun L, Wang H, Wang Z, He S, Chen S, Liao D, Wang L, Yan J, Liu W, Lei X *et al* (2012) Mixed lineage kinase domain-like protein mediates necrosis signaling downstream of RIP3 kinase. *Cell* 148: 213 – 227

Varfolomeev E, Blankenship JW, Wayson SM, Fedorova AV, Kayagaki N, Garg P, Zobel K, Dynek JN, Elliott LO, Wallweber HJ *et al* (2007) IAP antagonists induce autoubiquitination of c-IAPs, NF-kappaB activation, and TNFalpha-dependent apoptosis. *Cell* 131: 669 – 681

Varfolomeev E, Goncharov T, Fedorova AV, Dynek JN, Zobel K, Deshayes K, Fairbrother WJ, Vucic D (2008) c-IAP1 and c-IAP2 are critical mediators of tumor necrosis factor alpha (TNFalpha)-induced NF-kappaB activation. *J Biol Chem* 283: 24295 – 24299

Vince JE, Wong WW, Khan N, Feltham R, Chau D, Ahmed AU, Benetatos CA, Chunduru SK, Condon SM, McKinlay M *et al* (2007) IAP antagonists target cIAP1 to induce TNFalpha-dependent apoptosis. *Cell* 131: 682 – 693

Wallach D, Kang TB, Dillon CP, Green DR (2016) Programmed necrosis in inflammation: toward identification of the effector molecules. *Science* 352: aaf2154

Wan J, Block S, Scribano CM, Thiry R, Esbona K, Audhya A, Weaver BA (2019) Mad1 destabilizes p53 by preventing PML from sequestering MDM2. *Nat Commun* 10: 1540

Wang H, Sun L, Su L, Rizo J, Liu L, Wang LF, Wang FS, Wang X (2014) Mixed lineage kinase domain-like protein MLKL causes necrotic membrane disruption upon phosphorylation by RIP3. *Mol Cell* 54: 133 – 146

Wang T, Jin Y, Yang W, Zhang L, Jin X, Liu X, He Y, Li X (2017a) Necroptosis in cancer: an angel or a demon? *Tumour Biol* 39: 1010428317711539

Wang Y-T, Chen J, Chang C-W, Jen J, Huang T-Y, Chen C-M, Shen R, Liang S-Y, Cheng I-C, Yang S-C *et al* (2017b) Ubiquitination of tumor suppressor PML regulates prometastatic and immunosuppressive tumor microenvironment. *J Clin Invest* 127: 2982 – 2997

Wang ZG, Ruggero D, Ronchetti S, Zhong S, Gaboli M, Rivi R, Pandolfi PP (1998) PML is essential for multiple apoptotic pathways. *Nat Genet* 20: 266 – 272

Weinlich R, Oberst A, Beere HM, Green DR (2017) Necroptosis in development, inflammation and disease. *Nat Rev Mol Cell Biol* 18: 127 – 136

Wolyniec K, Carney DA, Haupt S, Haupt Y (2013) New strategies to direct therapeutic targeting of PML to treat cancers. *Front Oncol* 3: 124

Wu WS, Vallian S, Seto E, Yang WM, Edmondson D, Roth S, Chang KS (2001) The growth suppressor PML represses transcription by functionally and physically interacting with histone deacetylases. *Mol Cell Biol* 21: 2259 – 2268

Wu WS, Xu ZX, Ran R, Meng F, Chang KS (2002) Promyelocytic leukemia protein PML inhibits Nur77-mediated transcription through specific functional interactions. *Oncogene* 21: 3925 – 3933

Wu WS, Xu ZX, Hittelman WN, Salomoni P, Pandolfi PP, Chang KS (2003) Promyelocytic leukemia protein sensitizes tumor necrosis factor alpha-induced apoptosis by inhibiting the NF-kappaB survival pathway. *J Biol Chem* 278: 12294 – 12304

Zhang DW, Shao J, Lin J, Zhang N, Lu BJ, Lin SC, Dong MQ, Han J (2009) RIP3, an energy metabolism regulator that switches TNF-induced cell death from apoptosis to necrosis. *Science* 325: 332 – 336

Zhang H, Zhou X, McQuade T, Li J, Chan FK, Zhang J (2011) Functional complementation between FADD and RIP1 in embryos and lymphocytes. *Nature* 471: 373 – 376

Zhao J, Jitkaew S, Cai Z, Choksi S, Li Q, Luo J, Liu ZG (2012) Mixed lineage kinase domain-like is a key receptor interacting protein 3 downstream component of TNF-induced necrosis. *Proc Natl Acad Sci USA* 109: 5322 – 5327

Zhong S, Salomoni P, Pandolfi PP (2000) The transcriptional role of PML and the nuclear body. *Nat Cell Biol* 2: E85 – 90